NUREG/CR-3918
PNL-5186

Evaluation of Welded and Repair-Welded Stainless Steel for Light Water Reactor(LWR)Service

Compositional Effects on the Sensitization of Austenitic Stainless Steels

Prepared by S. M. Bruemmer, L. A. Charlot, D. G. Atteridge

Pacific Northwest Laboratory

**Prepared for
U.S. Nuclear Regulatory
Commission**

GPO Printed copy price: $4.50

NUREG/CR-3918
PNL-5186
R5

Evaluation of Welded and Repair-Welded Stainless Steel for Light Water Reactor(LWR)Service

Compositional Effects on the Sensitization of Austenitic Stainless Steels

Manuscript Completed: September 1984
Date Published: December 1984

S. M. Bruemmer, L. A. Charlot, D. G. Atteridge

Pacific Northwest Laboratory
Richland, WA 99352

Prepared for
Division of Engineering Technology
Office of Nuclear Regulatory Research
U.S. Nuclear Regulatory Commission
Washington, D.C. 20555
NRC FIN B2449

ABSTRACT

Pacific Northwest Laboratory is conducting a program, sponsored by the U.S. Nuclear Regulatory Commission, to develop validated models for the prediction of stress corrosion cracking susceptibility in the heat-affected zone of stainless steel weldments. This report reviews the effects of alloying and impurity elements on the sensitization propensity of Types 304 and 316 stainless steel. As expected, carbon was found to be the dominant element controlling sensitization, with chromium, molybdenum, and nickel also important. Other alloying elements, such as manganese and silicon, have at most only a small effect on sensitization. However, strongly segregating elements, such as nitrogen, boron, and phosphorus, may have a significant effect on intergranular corrosion and stress corrosion cracking susceptibility.

SUMMARY

Pacific Northwest Laboratory is conducting a program, sponsored by the U.S. Nuclear Regulatory Commission, to develop validated models for the prediction of stress corrosion cracking susceptibility in the heat-affected zone of stainless steel weldments. This report reviews the effects of specific alloying and impurity elements on the sensitization of Types 304 and 316 stainless steels. Basic understanding of the sensitization phenomenon is developed by examination of the thermodynamics and kinetics of carbide precipitation and chromium depletion. Individual elemental effects are isolated and discussed. Methods to predict material sensitization are reviewed and assessed by comparison to a large isothermal sensitization data base. In addition, several aspects of austenitic stainless steel metallurgy which do not directly affect sensitization have been analyzed because they may have a significant effect on stress corrosion cracking susceptibility.

Bulk carbon content is the dominant factor controlling sensitization. Reducing the carbon concentration significantly decreases the steel's susceptibility to sensitization and intergranular stress corrosion cracking (IGSCC). Low ($\leq$0.02 wt%) carbon stainless steels are extremely resistant to sensitization during proper welding practices. Other alloying elements, such as molybdenum, chromium, and nickel have a strong effect on carbon and chromium activities and thereby on sensitization. These elements must be taken into account when assessing a material's resistance to sensitization.

Methods to determine the relative sensitization resistance of particular stainless steel heats as a function of bulk composition have been reviewed and compared to a large data base. The best predictive capability was obtained by normalizing the chromium content as a function of molybdenum, nickel, and carbon contents to calculate a composite chromium (Cr*) value:

$$Cr^* = Cr + 1.6\ Mo - 0.2\ Ni - 100\ C$$

where the elements listed represent their bulk concentration in weight percent. Other elements such as manganese, silicon, and nitrogen were evaluated but did not significantly improve the predictive capability.

A positive correlation between prediction and experimental data was documented, enabling the estimation of improvement factors based on time required for sensitization to occur. A simple method to determine factors of improvement is proposed based on this correlation. These factors allow materials to be compared and assessed in reference to their expected sensitization resistance based on bulk composition information. A factor of improvement of approximately 20 times is predicted comparing nuclear grade Type 316 stainless steel to a typical Type 304 stainless steel.

Classical sensitization resulting from grain boundary chromium depletion is the primary, but not the only, reason for a stainless steel's susceptibility to intergranular corrosion and SCC. Phosphorus, sulfur and silicon can promote intergranular attack in certain environments and may contribute to IGSCC. Impurity elements such as sulfur and phosphorus enrich grain boundary regions by factors more than 10^4 times their bulk concentration. Nitrogen and boron also strongly segregate to grain boundaries and may have a significant effect on corrosion and SCC susceptibility. Lowering the bulk carbon concentration in alloys such as the nuclear grade stainless steels may increase the importance of impurity elements since the potential for sensitization is significantly reduced. Additional understanding of impurity element effects is required to determine whether the nuclear grade alloys are immune to IGSCC in boiling-water reactor (BWR) environments.

CONTENTS

FIGURES

TABLES

1.0 INTRODUCTION

1.1 BACKGROUND

Austenitic stainless steel (SS) is susceptible to intergranular stress corrosion cracking (IGSCC) when exposed to a sufficiently severe combination of a sensitized microstructure, aggressive environment, and stress level. This review will consider the first of these conditions in detail. It is important to keep in mind, however, that a sensitized microstructure alone is not sufficient to promote cracking. Thus, adequate understanding and control of all three conditions is required to ensure resistance to IGSCC.

The objectives of this report are to review what is known about the effects of material composition on sensitization development and to present both empirical and theoretical methods to compare a material's propensity to sensitize. The primary data base for this review is isothermal sensitization results and cannot be directly applied to predict weld-induced sensitization. Simultaneous strain during the welding thermal cycle is known to have a significant effect on sensitization development and susceptibility to IGSCC. However, while the kinetics of sensitization may change with simultaneous straining, the basic effects of bulk composition on carbide precipitation and chromium depletion are the same. Therefore, isothermal data can be used to indicate, at least qualitatively, the weld-induced compositional effects on degree of sensitization (DOS) and IGSCC susceptibility.

Sensitization refers to the loss of corrosion resistance after heat treatment in, or slow cooling through, a particular temperature regime. This susceptibility to corrosion results from a change in the local composition at grain boundaries. The primary composition change that occurs is the precipitation of chromium-rich carbides and an associated depletion of chromium in the adjacent region. The importance of chromium depletion was first proposed by Bain, Aborn, and Rutherford[1] and was more quantitatively developed by Stawström and Hillert[2] and Tedmon et al.[3] Experimental measurements[4-6] have indicated that the chromium-depleted zone is, in most cases, directly responsible for the loss in intergranular corrosion (and stress corrosion) resistance.

The development of a sensitized microstructure is controlled by the thermodynamics of carbide formation and the kinetics of chromium diffusion. Sensitization occurs in a temperature regime in which chromium carbides are thermodynamically stable ($\leq$850°C) and chromium diffusion is sufficiently rapid ($\geq$500°C) so that precipitates can form in a reasonable period of time. If chromium diffusion occurs too rapidly (>800°C), precipitates will form, but no significant chromium depletion will result. Therefore, sensitization only

results from thermal exposure within a relatively narrow temperature range. This range is normally between 500 and 800°C but is strongly dependent on material composition.

1.2 RESEARCH PROGRAM

This review is the first in a series of reports assessing methods to predict stress corrosion cracking (SCC) susceptibility of the heat-affected zone (HAZ) in austenitic stainless steel weldments. It has been prepared as part of the program "Evaluation of Welded and Repair-Welded Stainless Steel for LWR Service" being conducted by Pacific Northwest Laboratory[a] for the U.S. Nuclear Regulatory Commission (NRC). The primary objective of this program is to develop and validate methods for the component-specific prediction of SCC susceptibility in nuclear reactor water environments.

The final assessment method will consider the effects of material composition, thermomechanical history, and reactor operating parameters. It will enable the prediction of component SCC susceptibility as a function of reactor life and will be applicable to as-fabricated and repair-welded components with prior service history. Model predictions will be used to assist in decisions concerning component replacement and to help specify allowable repair-welding conditions.

This report reviews the effects of alloying and impurity elements on the isothermal sensitization of Types 304 and 316 SS and assesses several methods to correlate the effects of individual elements. Such a correlation is critical to the development of an accurate prediction method for SCC susceptibility.

(a) Operated for the U.S. Department of Energy by Battelle Memorial Institute.

2.0 CARBIDE PRECIPITATION IN AUSTENITIC STAINLESS STEELS

Heat treatment of austenitic stainless steels in the temperature range from 500 to 850°C leads to precipitation and growth of chromium-rich carbides at grain boundaries. Regions adjacent to these precipitates may become depleted in chromium and thus susceptible to corrosive attack. The formation of chromium-rich carbides depends on the amount of carbon available (a function of the carbon bulk concentration, activity, and solubility), the phase equilibrium established between particle and matrix, and the rate of carbon and chromium arrival at some nucleation and growth site. The following sections present published materials data relevant to chromium-rich carbide formation in austenitic stainless steels as these data relate to the process of sensitization. While carbide precipitation and chromium depletion are the primary cause of sensitization, the precipitation of other second phases can also lead to corrosion in certain environments and will, therefore, be discussed as well.

2.1 DIFFUSION OF CARBON AND CHROMIUM

The rate-controlling step in the sensitization of austenitic stainless steels is, in most cases, the diffusion of chromium to the grain boundary. Diffusivity values for carbon in the steels are several orders of magnitude greater than for chromium; consequently, the carbon gradient within the alloy grain structure can be considered very small. The net effect is that at some sensitizing temperature the carbon content will decrease fairly uniformly in the alloy over time. The chromium concentration within the grain, however, will remain near the initial concentration, with a steep concentration gradient occurring at the grain boundary. A minimum chromium concentration at the carbide/matrix interface will be defined primarily by the carbon activity. The diffusion of chromium and the local chromium equilibrium at the carbide/austenite interface form the basis of the chromium depletion theory of intergranular corrosion susceptibility. This theory will be discussed in more detail in Section 4.3.

Volume or lattice diffusivity values for chromium and carbon in austenitic steels have been reported by several investigators. Within the temperature range normally conducive to sensitization, the diffusion of chromium and carbon in Types 304 and 316 SS can be calculated from the following equations:

304 SS:	$D_{Cr} = 0.08 \exp(-58500/RT)$	Reference 2	(1)
316 SS:	$D_{Cr} = 0.334 \exp(-63900/RT)$	Reference 7	(2)
304 SS:	$D_{C} = 6.18 \exp(-22450/RT)$	Reference 8	(3)
316 SS:	$D_{C} = 0.19 \exp(-18820/RT)$	Reference 8	(4)

Calculations of typical diffusivities in Type 304 SS at 650°C illustrate the significant disparity between chromium (1.1×10^{-15} cm/s) and carbon (1.6×10^{-10} cm/s). This difference prompts the formation of the chromium-depleted zone during sensitization.

2.2 SOLUBILITY OF CARBON

Carbide precipitation results from an excess or supersaturation of carbon in the austenitic alloy following high-temperature heat treatment. Thermal treatment of the alloy in or through the sensitizing temperature range establishes the equilibrium between carbon in solid solution and carbon tied to carbide particles. The temperature dependence of chromium carbide precipitation is shown in Figure 2.1 for a 300 series-type stainless steel.

The horizontal dashed line in Figure 2.1 indicates the total amount of carbon in the alloy. The difference between the horizontal dashed line and the solid line is the maximum equilibrium amount of carbon in solid solution as a function of temperature, with a decrease in carbon solubility first appearing around 980°C. The curved dashed lines contained in the insoluble carbon region illustrate the effect of time and temperature on carbide precipitation. Equilibrium is achieved only at relatively long times at high temperatures (e.g., on the order of 15 h at 800°C and 150 h at 700°C). Thus, while the equilibrium amount of carbon in solid solution decreases with decreasing temperature, the time required for carbide precipitation increases significantly and equilibrium will not achieved under practical conditions below about 600°C.

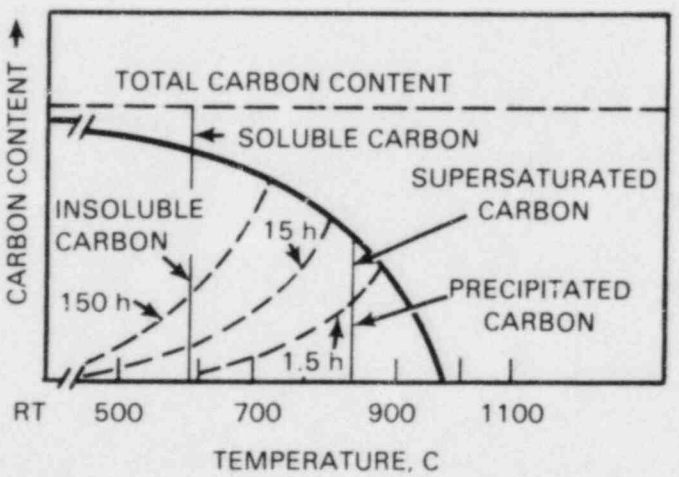

FIGURE 2.1. Precipitation Diagram for Typical 300 Series Stainless Steel[9]

Carbide precipitation in the sensitization range can be explained by a mass balance approach (from Figure 2.1), given by

$$C(T) = C_1 - C_T - S_C(T) \quad (4)$$

where $C(T)$ = amount of excess carbon at temperature (T)
C_1 = total carbon in the alloy
C_T = carbon trapped as carbides at some previously higher temperature heat treatment
$S_C(T)$ = terminal solubility of carbon at temperature (T).

The effects of time and temperature show that the precipitation process depends on the availability of carbon and requires sufficient time at temperature for nucleation and growth to occur.

The terminal solubility of carbon in austenitic steels as a function of temperature has been reported by Arioka et al.[7] as

$$S_C(wt\%) = 2527.7 \exp(-24805/RT) \quad (5)$$

from the data of Bain, Aborn, and Rutherford.[1] Natesan and Kassner[10] determined a similar relationship to describe carbon solubility in an Fe-18Cr-8Ni alloy:

$$S_C(wt\%) = 1088 \exp(-23653/RT) \quad (6)$$

Both of these expressions give comparable predictions for the interrelationship between temperature and carbon solubility, as shown in Figure 2.2. The solubility limit is exceeded in a 0.06 wt% alloy below ~900°C and in a 0.02 wt% alloy below ~800°C. This illustrates that the driving force still exists for carbide precipitation even in low-carbon materials.

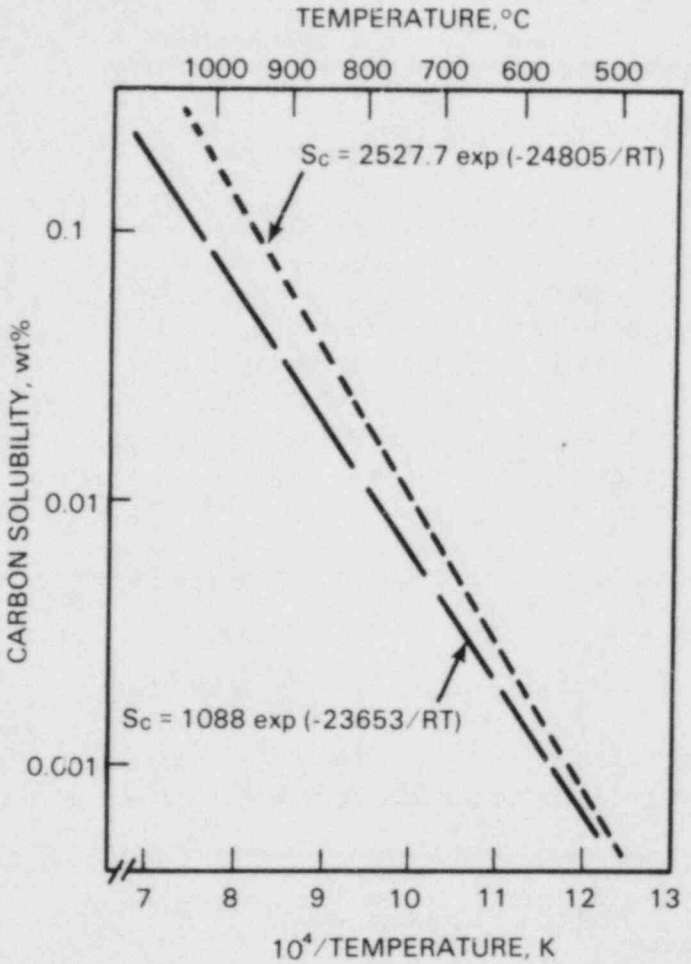

FIGURE 2.2. Temperature Dependence of Carbon Solubility in 300 Series Stainless Steels

2.3 THERMODYNAMICS OF CARBIDE FORMATION

The susceptibility of austenitic stainless steel to intergranular corrosion and SCC depends on the depth and width of the chromium-depleted zone. In order to predict the minimum chromium content associated with the nucleated carbides, it is necessary to understand the precipitation thermodynamics to some extent. The thermodynamic stability of the carbide depends primarily on the activity of the chromium and carbon. Assuming the simple $Cr_{23}C_6$ carbide, the equilibrium condition necessary to maintain a carbide is given by

$$K_{eq}^{T} = \exp(-\Delta F/RT) = (a_{Cr_{23}C_6})/(a_{Cr})^{23}(a_C)^6 \qquad (7)$$

where K_{eq}^{T} is the equilibrium constant, ΔF is the change in free energy; the activities of the carbide, Cr, and C are given by $aCr_{23}C_6$, a_{Cr}, and a_C, respectively. By replacing the activity terms with composition terms, i.e., $a_i = \gamma_i X_i$ (γ is the activity coefficient and X is the mole fraction), the expression can be written to determine the chromium concentration (X_{Cr}) in equilibrium with the carbide at a constant temperature:

$$X_{Cr} = (1/K_{eq})^{1/23} (\gamma_{Cr}) (\gamma_C X_C)^{6/23} \tag{8}$$

Tedmon et al.[3] have used this thermodynamic approach to explain sensitization based upon the chromium-carbon equilibrium and minimum chromium concentrations at the grain boundaries of austenitic stainless steels. The two primary factors in the quantitative analysis are, as indicated above, the carbon and chromium activity coefficients. The former was obtained from a simplied series expansion:

$$\ln\gamma_C = \ln\gamma_C^{0} + X_C \left(\frac{\partial \ln\gamma C}{\partial X_C}\right) + X_{Ni} \left(\frac{\partial \ln\gamma C}{\partial X_{Cr}}\right) \tag{9}$$

and the latter, treated as an adjustable parameter, was obtained from corrosion data. The influence of chromium, which greatly lowers the carbon activity coefficient, and of nickel, which increases it, are shown in Figures 2.3a and b. The effect of bulk chromium content on the chromium activity coefficient in austenitic stainless steels is displayed in Figure 2.3c.

The assumption of a pure chromium carbide and regular solution temperature dependence is in contradiction to experiment, where complex carbides in Type 316 SS and Fe-Cr carbides in Type 304 SS have been found. The presence of additional carbide-forming elements (besides chromium) in complex carbides may have a significant effect on carbon and chromium activities and, therefore, on sensitization. Fullman[11] applied the thermodynamics of carbide formation to predict the influence of metallic elements other than chromium on sensitization and IGSCC susceptibility in stainless steels. Thermodynamic data on Fe-Cr-Ni-M-C interactions were used to estimate the chromium concentration in equilibrium with a complex $(Fe,Cr,Ni,M)_{23}C_6$ carbide. Partial molar free energies, using ideal solution approximations, were taken from a number of sources to describe the thermochemistry of $(Fe_ICr_J)_{23}C_6$ and $(Fe_ICr_JM_K)_{23}C_6$ carbides (I, J, and K are constants). The free energies of binary carbides ($M_{23}C_6$) were determined from thermochemical data on stable carbides or from a series of stable carbides. It was often necessary to estimate a value relevant for a $M_{23}C_6$-type carbide. This approach allowed comparison of elemental effects on

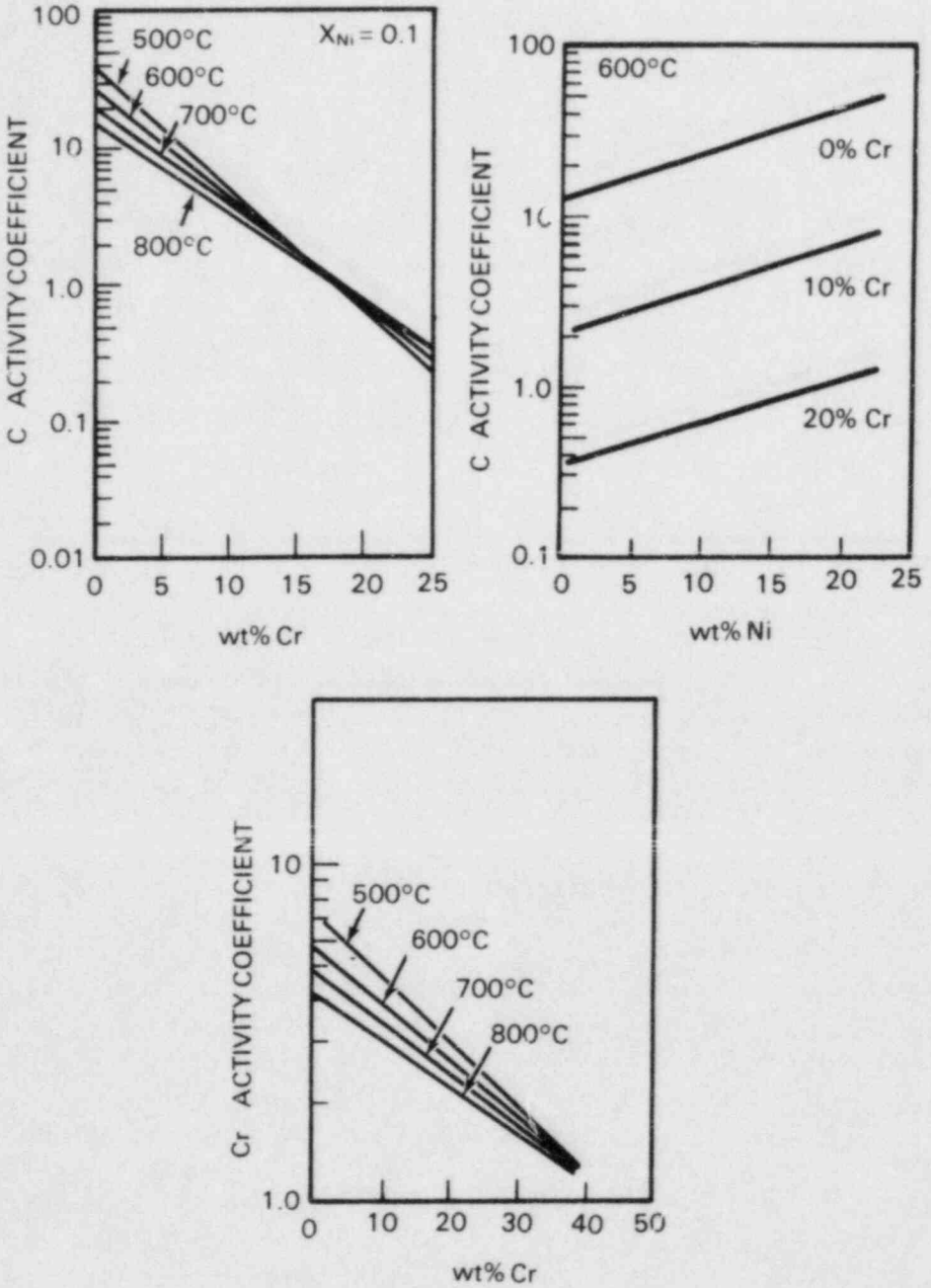

FIGURE 2.3. Bulk Composition Effects on Activity Coefficients in Austenitic Stainless Steels: (a) carbon activity versus chromium content; (b) carbon activity versus nickel content; and (c) chromium activity versus chromium content.(3)

carbide formation and, therefore, the minimum chromium content adjacent to the carbide. Prediction of elemental effects on sensitization using Fullman's derived parameters is discussed in Section 4.1.

2.4 PRECIPITATE PHASES

The predominant carbide found in stainless steels is the $M_{23}C_6$ (fcc) carbide. In Type 304 SS, this precipitate is a chromium-rich carbide of $(Cr_{0.77}Fe_{0.2}Ni_{0.03})_{23}C_6$.[12] Precipitation of the carbide is a function of thermal treatment (time and temperature) and the bulk carbon content of the alloy. The onset of precipitation in a particular alloy can be described by time/temperature/precipitation diagrams as shown in Figure 2.4. Also shown in this figure are the preferred precipitation sites in a Type 304 SS alloy. Carbide precipitation occurs first at the delta ferrite/austenitic interface, then at the austenite grain boundaries, along incoherent twin boundaries, and finally at coherent twin boundaries. This general course of precipitation has been shown in duplex alloys,[13] Type 316 SS alloys,[14] and high-chromium austenitic steels[13] as well.

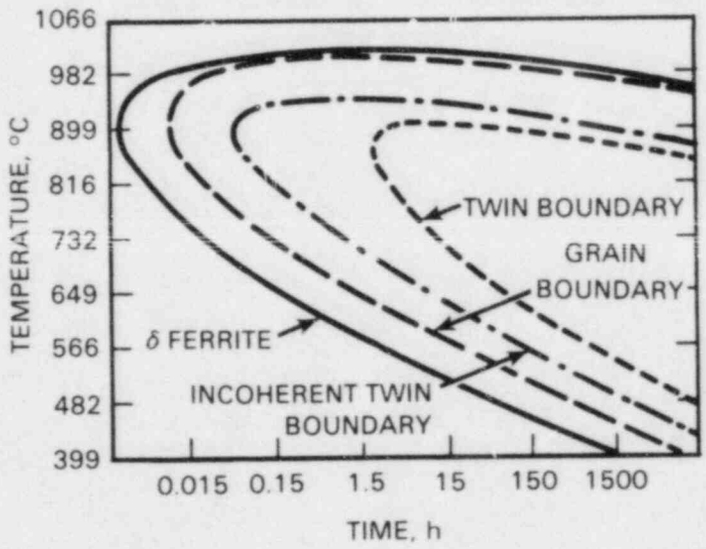

FIGURE 2.4. Time/Temperature Dependence of $M_{23}C_6$ Precipitation in Type 304 Stainless Steel with 0.038% C[9]

The carbide precipitates that do form can be classified as two-dimensional, submicroscopic particles; as dendrites, which will be initially lamellar in form; or as small geometric particles. The temperature dependence of

the precipitate type is shown in Figure 2.5. Crystallographic developed carbides are not necessary for intergranular corrosion; networks of thin sheets or dendrites have been found in alloys showing intergranular attack.[15]

In addition to the primary phases, several other precipitates can form during heat treatment. This is particularly true for Type 316 SS in comparison to Type 304 SS. The effect of carbon on the precipitation phase in Types 316 and 316L SS is shown in Figure 2.6. The dominant carbide (as for Type 304 SS) is the $M_{23}C_6$ phase whereas the intermetallics (including sigma, chi, and Laves phases) are more apt to form at low carbon contents. Under some conditions (e.g., in low-carbon, highly strained regions or in low-carbon, nitrogen-doped alloys), martensite may also be present in the austenitic alloy. The presence of these other second phases may contribute to IGSCC susceptibility, but not to the degree of sensitization. There is insufficient chromium enrichment in these second phases to cause a chromium-depleted region to form in the adjacent matrix.

The crystal structures and compositions of phases that have been observed in Type 316 SS are listed in Table 2.1. Of these phases, sigma has been shown to promote intergranular attack in certain oxidizing media, but not in tests relevant to high-temperature water environments. Other intermetallic phases have not been observed to increase susceptibility to corrosion. The characteristics of the second phases found in Type 316 SS have been recently reviewed by Lai[16] and will not be considered in more detail here. There does appear to be a need for better characterization of precipitates in low-carbon, relatively high-nitrogen materials (e.g., nuclear grade Type 316 SS).

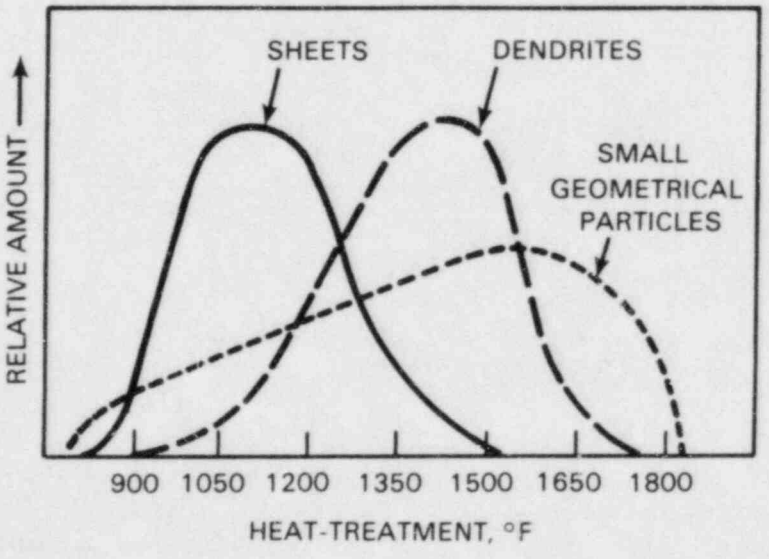

FIGURE 2.5. Temperature Dependence of Morphology for Grain-Boundary Carbides[15]

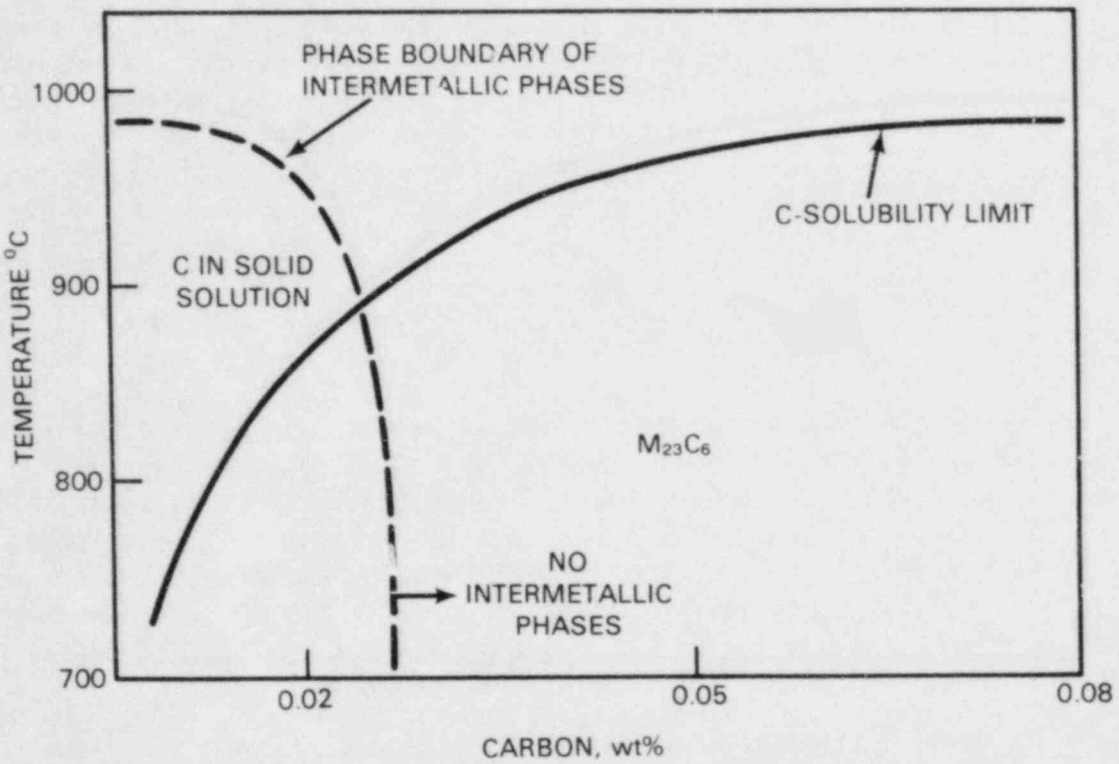

FIGURE 2.6. Stability Ranges of Carbides and Intermetallic Phases in Type 316 SS as a Function of Bulk Carbon Content

TABLE 2.1. Crystal Structure and Composition of Phases in Aged Types 316L and 316 Stainless Steels[16]

Phase	Crystal Structure	Composition, wt%			
		Mo	Cr	Fe	Ni
$M_{23}C_6$	fcc	14	63	18	5
M_4C	fcc				
Sigma (σ)	Tetragonal	11	29	55	5
Chi (χ)	bcc α-Mn structure	22	21	52	5
Laves (η)	Hexagonal	45	11	38	6

The effect of martensite on the corrosion and SCC susceptibility has received considerable attention in recent years and merits some discussion.

Unstabilized austenitic stainless steels may partially transform to α' martensite as a result of room-temperature plastic deformation. Temperature, extent of deformation, and bulk material composition all influence the amount of martensite that will form. Empirical relationships that estimate the martensite formation temperature (M_s) from the composition of alloying elements in solution in austenite have been proposed by Eichelman and Hull[17] and Monkman et al.[18] The Eichelman and Hall equation considers more elements and can be expressed[19] as

$$M_s[°K] = 1578 - 41.7\ Cr - 61.6\ Ni - 33.3\ Mn - 27.8\ Si - 36.1\ Mo - 1667(C+N) \quad (10)$$

where the element designations represent their weight percent in solution in the austenite phase. An immediate observation is that the M_s temperature increases with decreasing alloying element concentrations. A typical Type 304 SS alloy would be expected to have a transformation temperature of about -150°C. However, in a sensitized grain boundary with depleted chromium levels, the predicted M_s temperature rises above room temperature, and martensite may form preferentially in these regions. Such localized martensite nucleation has been documented by several investigators.[20,21]

The presence of martensite in Type 304 SS has been shown to accelerate corrosion susceptibility.[22-24] Attack morphology was transgranular, resulting from carbide precipitation (and apparently chromium depletion) within martensite laths. Sensitization developed much more rapidly (particularly at low temperatures) because of the increased diffusion of chromium and carbon in the martensite.[22] Fewer data are available concerning the effect of preferential martensite formation along grain boundaries, which has been implicated in the hydrogen embrittlement of austenitic stainless steels,[25] but has not been studied extensively in reference to dissolution processes.

3.0 INDIVIDUAL ELEMENT EFFECTS ON SENSITIZATION

Sensitization of austenitic stainless steels requires the precipitation of chromium-rich carbides along grain boundaries. Thus, it is not surprising that carbon and chromium are the predominant compositional variables controlling this phenomenon. Although both elements are critical, the propensity of a material to sensitize can often be inferred simply from the carbon content, mainly because of the wide range of carbon compositions (0.01 to 0.08 wt%) that are possible in Types 304 and 316 stainless steels. Chromium content, on the other hand, is specified within a much narrower band (18 to 20 wt% for 304 SS or 16 to 18 wt% for 316 SS) in these alloys.

Time/temperature/sensitization curves such as those in Figure 3.1 have been used for many years to estimate the susceptibility of a particular heat to intergranular corrosion and SCC. The "nose" of the time-temperature-sensitization curve specifies the minimum time required for sensitization. This minimum value is dependent on material composition. Offsetting the "nose"

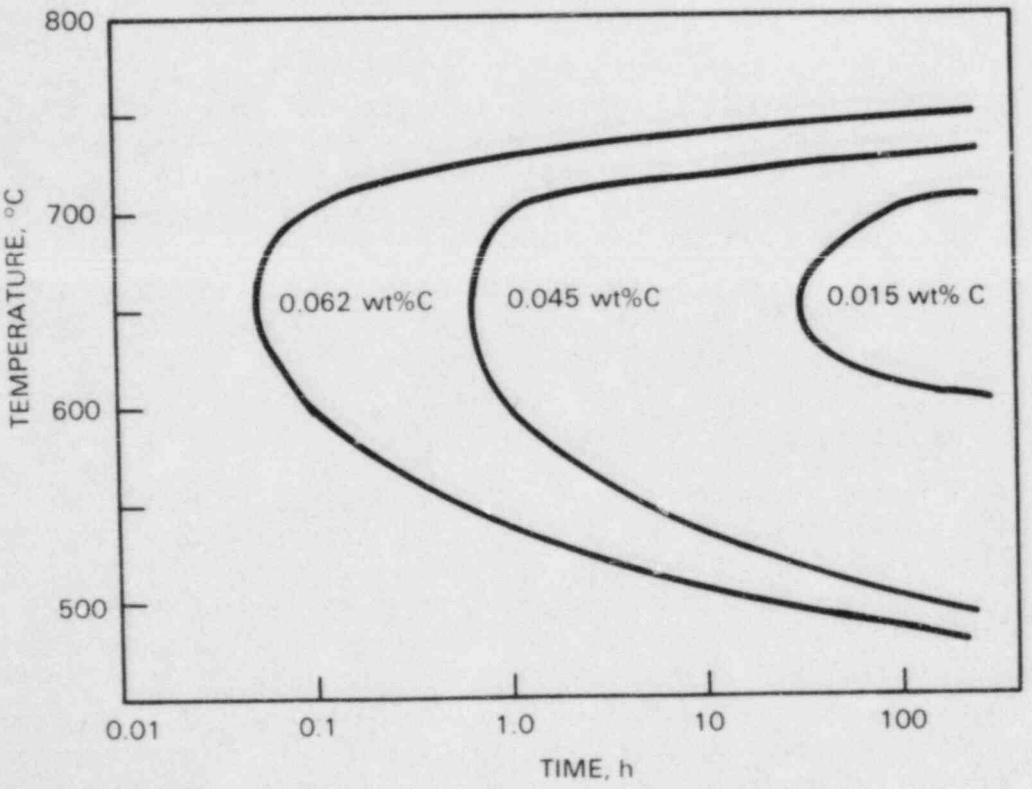

FIGURE 3.1. Time/Temperature/Sensitization Curves Determined by Electrochemical Potentiokinetic Reactivation (EPR) Tests on Type 304 SS Alloys of Variable Carbon Contents[26]

to longer times decreases the probability that sensitization will occur during actual fabrication (e.g., welding). Direct correlations between time-to-sensitize measurements and composition-based terms allow the effect of specific elements to be examined. We will employ this method of comparison because of the large data base of available time/temperature/sensitization curves.[27-57] These time-to-sensitize measurements are dependent on both the thermodynamics and kinetics of the precipitation/depletion phenomenon. As a result, some scatter will occur due to differences in the initial microstructural conditions of the many heats, and due to the attempt to correlate the evaluation test results of numerous experimentors.

3.1 CARBON

The strong dependence of sensitization and IGSCC susceptibility on bulk carbon content has been recognized for more than 50 years. Time/temperature/sensitization curves illustrate this dependence (Figure 3.1). The curves summarize the time/temperature conditions required for sensitization as a function of bulk carbon content. Increasing the carbon content from 0.015 to 0.062 wt% sharply decreases the time required for sensitization at temperatures between 550°C and 750°C.[26]

The excellent correlation between time-to-sensitize and bulk carbon content for Type 304 SS shown in Figure 3.2a indicates not only the critical importance of carbon but the secondary importance of other elements in this alloy. No other element shows a positive correlation without factoring in the overriding effect of carbon. The importance of other alloying elements becomes obvious when time-to-sensitize measurements for Type 316 SS are added to the data base, as shown in Figure 3.2b. The wide scatter in the data results from significant differences in chromium, molybdenum and nickel concentrations between individual Type 304 and 316 SS alloys

3.2 MAJOR ALLOYING ELEMENTS

Considerable empirical and theoretical evidence exists to document the influence of alloying elements such as chromium, nickel and molybdenum on the sensitization and IGSCC susceptibility of austenitic stainless steels. Chromium has a pronounced effect on the passivation characteristics of stainless steels. Decreasing the chromium content below about 13 wt% destabilizes the passive film (Figure 3.3a) and sharply increases the dissolution rate (Figure 3.3b). This is perhaps the best evidence that chromium depletion controls the intergranular corrosion of stainless steels. Thus, local chromium depleted regions are likely sites (relative to the matrix) for dissolution. It is postulated that bulk chromium levels have an effect on corrosion susceptibility by determining the magnitude of local depletion that can be tolerated before reaching the critical chromium level and that alloys with higher chromium

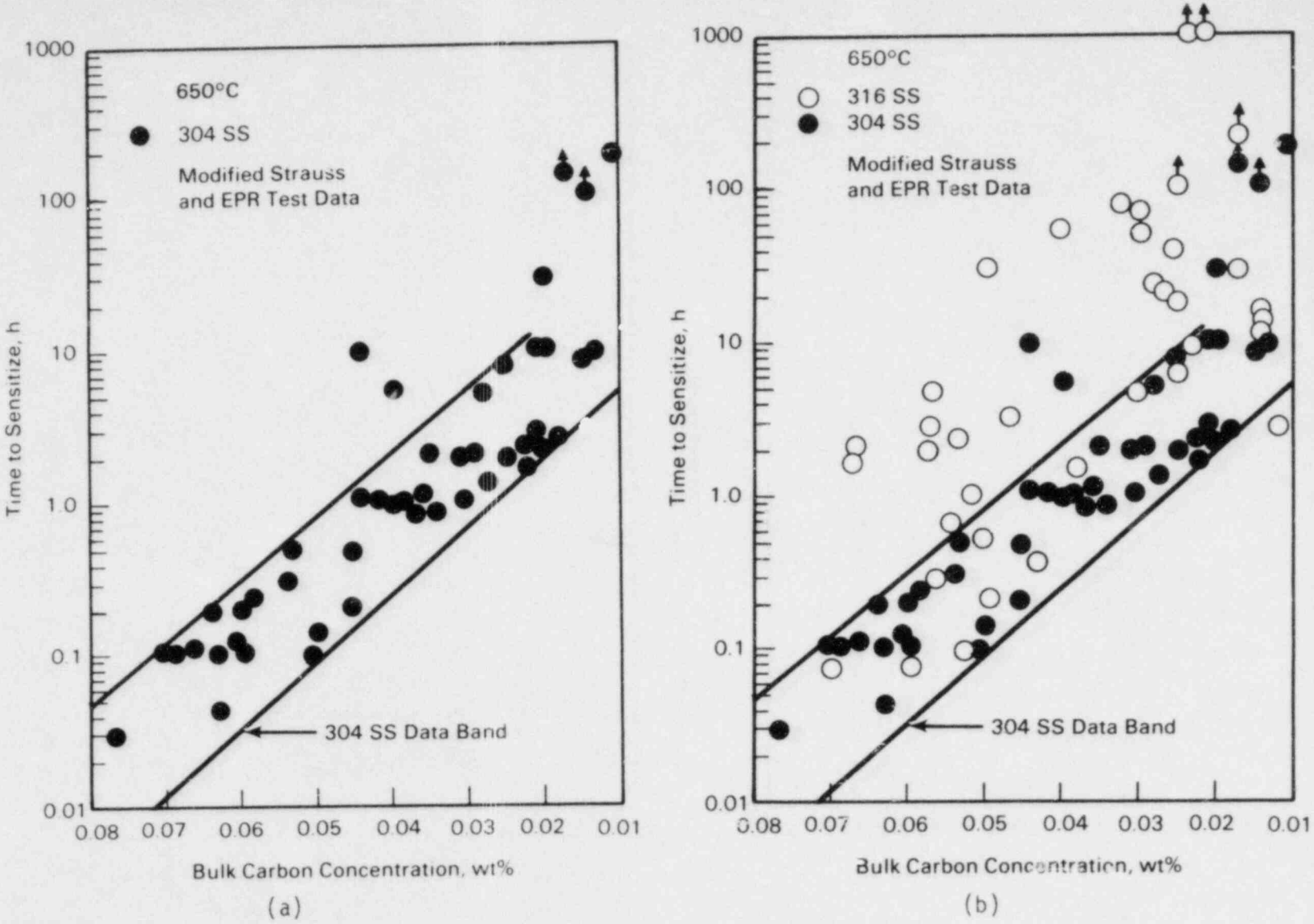

FIGURE 3.2. Time-to-Sensitize Data as Determined by Modified Strauss or EPR Tests at 650°C Plotted as a Function of Bulk Carbon Content for (a) Type 304 SS and (b) with Data for Type 316 SS Included

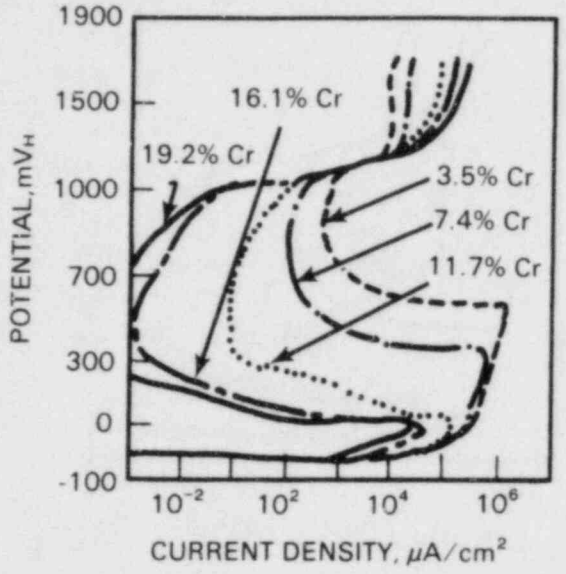

(a)

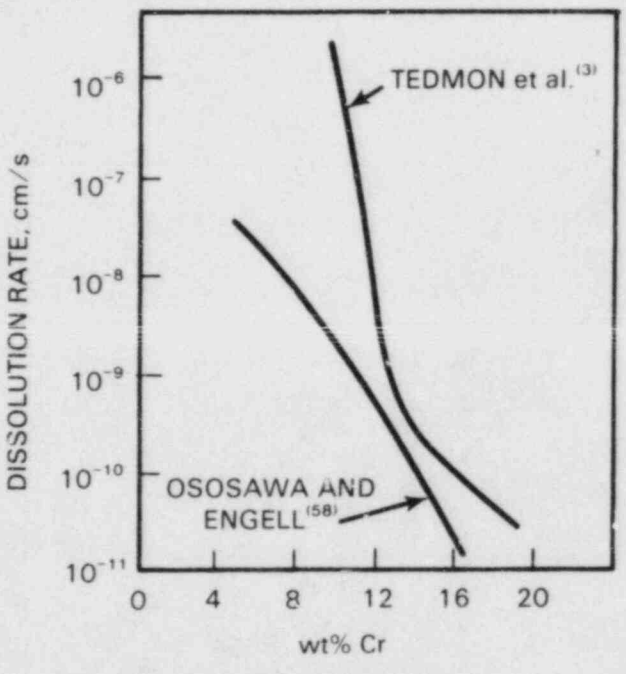

(b)

FIGURE 3.3. Polarization Curves (a) and Bulk Dissolution Rates (b) for Fe-10% Ni Alloys as a Function of Chromium Concentration

levels would be more resistant to sensitization. However, very little well controlled data exist to corroborate this hypothesis.

Molybdenum has an effect on sensitization development similar to that of chromium. It is incorporated into carbide precipitates along grain boundaries, and the molybdenum remaining in solution contributes to the passivation process during corrosion. This element accounts for the greater resistance of Type 316 over Type 304 to intergranular corrosion and pitting corrosion. Molybdenum depletion at grain boundaries has also been observed in sensitized Type 316 SS,[28] further indicating the similar behavior of molybdenum and chromium. To correlate composition with IGSCC susceptibility of many stainless steels, Cihal[59] found it necessary to correct for molybdenum by using an "effective" chromium concentration.

The presence of molybdenum in Type 316 SS has been shown to promote the precipitation of a variety of other phases both in the matrix and along grain boundaries. At the present time, these phases (see Section 2.4 for a more complete description) do not appear to effect intergranular corrosion or SCC in pertinent environments. However, in more oxidizing environments (e.g., Huey test), sigma phase particles are rapidly attacked.

Nickel is required in austenitic stainless steels to stabilize the austenitic phase field and must be increased with increasing chromium concentrations. However, increasing the bulk nickel content decreases the solubility and increases the activity of carbon. As a result, nickel additions tend to exacerbate sensitization. A balance between carbon, chromium, and nickel concentrations to avoid sensitization was determined by Cihal[29] for Type 304 SS alloys. Higher levels of nickel sharply reduce the allowable carbon concentration to avoid sensitization. This correlation, shown in Figure 3.4, illustrates the interdependence of multiple composition variables on the development of sensitization.

Other alloying elements that are present in significant amounts in Types 304 and 316 SS are manganese, silicon, and nitrogen (in N, LN, and NG grades). Very few well controlled studies have been performed on the effect of manganese, even though a significant amount (~2.0 wt%) is specified in these materials. Manganese has been suggested to improve sensitization resistance by retarding chromium carbide formation,[13] and it does appear to contribute to the effect of nitrogen to inhibit carbide formation as measured by oxalic acid tests.[27] In contrast, comparison of Huey and Strauss test results on Types 201, 202, and 304 stainless steels showed that the higher-manganese Type 202 was slightly more susceptible to intergranular attack than the lower-manganese alloys.[60]

Silicon has been observed to promote intergranular corrosion of high-purity[61-62] and commercial-purity[63-65] stainless steels. Molybdenum-containing steels were found to be much more sensitive to silicon additions.

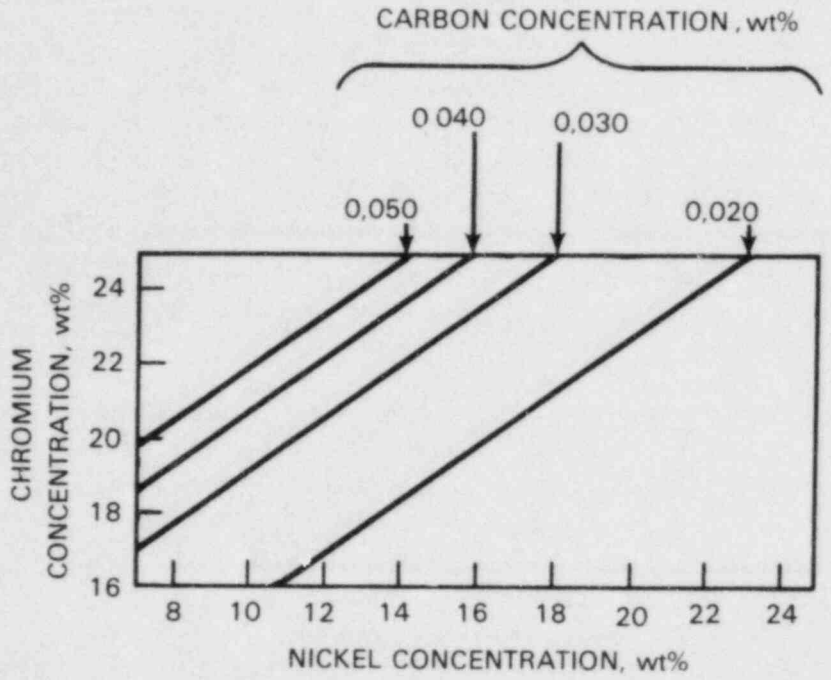

FIGURE 3.4. Interrelationship Between Chromium and Nickel Contents on the Carbon Content Required to Avoid Sensitization After 1-h Heat Treatment at 650°C[29]

Considerable evidence exists to indicate that segregation of silicon to grain boundaries induces intergranular attack, particularly in highly oxidizing solutions. In nonsensitized materials, this segregation appears to result from a nonequilibrium phenomenon leading to rather broad regions of silicon enrichment at the grain boundary.[63] This type of segregation will not be present in a sensitized microstructure. If silicon does influence sensitization, it must operate through equilibrium segregation or by affecting chromium and carbon activities.

One of the alloying additions most studied in recent years has been nitrogen. The effect of nitrogen on sensitization and IGSCC susceptibility is rather complex and is dependent on the presence of other alloying additions. More than 30 years ago, Binder et al.[43] observed intergranular attack in Type 304 SS only when it contained certain compositions of nitrogen and nickel. Much recent work[27,28,66] indicates that nitrogen content (<0.12 wt%) either has very little effect on sensitization or actually improves sensitization resistance by retarding the precipitation and growth of chromium carbides.[27] The presence of molybdenum and manganese in combination with nitrogen tends to further improve sensitization resistance.

The deleterious effect of carbon on sensitization can be reduced by additions of stabilizing elements, such as titanium and niobium. Both of these elements form more stable carbides than chromium and therefore limit the number of "sensitizing" carbides that precipitate. Stabilization is only effective when the Ti/C and Nb/C ratios are sufficiently large. Niobium additions appear to be more beneficial than titanium additions. Akashi and Kawamota[49] observed the following order of material resistance to IGSCC in high-temperature oxygenated water: 347 > 316L > 321 ~ 304L > 316 > 304. Stabilized grades are susceptible to weld HAZ cracking, commonly referred to as "knife-line attack." Knife-line attack is found mostly in oxidizing environments and probably results from some local chromium depletion, impurity segregation, and precipitation of intermetallics.

3.3 IMPURITY ELEMENTS - SEGREGATION

Although chromium depletion is the primary microstructural cause of sensitization, substantial evidence indicates that grain-boundary segregation of certain elements also contributes to intergranular corrosion and SCC susceptibility.[63,67-70] High-purity stainless steel heats have shown significant improvement over commercial heats in their resistance to intergranular attack.[71] Intergranular corrosion has also been observed in solution-annealed materials when no detectable precipitates were present. Nearly all of the intergranular corrosion tests that show these results have been observed in highly oxidizing solutions. Very little experimental data show a direct correlation between susceptibility and grain boundary segregation in more pertinent environments.

Impurity elements in a variety of materials have been observed to enrich grain boundaries at levels that are more than 10^4 times the bulk concentration. Thus, an element present in the bulk at only 10 ppm may reach a concentration of 10% in the interface region. Enrichments of this magnitude have been observed for sulfur and boron in both iron and nickel. A general interrelationship between grain boundary enrichment and atomic solid solubility has been demonstrated;[72] see Figure 3.5. Each of the enrichment ratios plotted in this figure result from direct measurements of grain boundary composition by surface analysis techniques (primarily Auger electron spectroscopy). An excellent review of grain boundary segregation principles and measurement has been published by Hondros and Seah.[72]

Joshi and Stein[63] reported the first data on grain boundary composition of an austenitic stainless steel, identifying many enriched elements including phosphorus, sulfur, silicon, and nitrogen. The most consistently measured impurity element has been phosphorus. Lumsden and Stocker[68] examined both equilibrium segregation levels and the kinetics to reach equilibrium for a

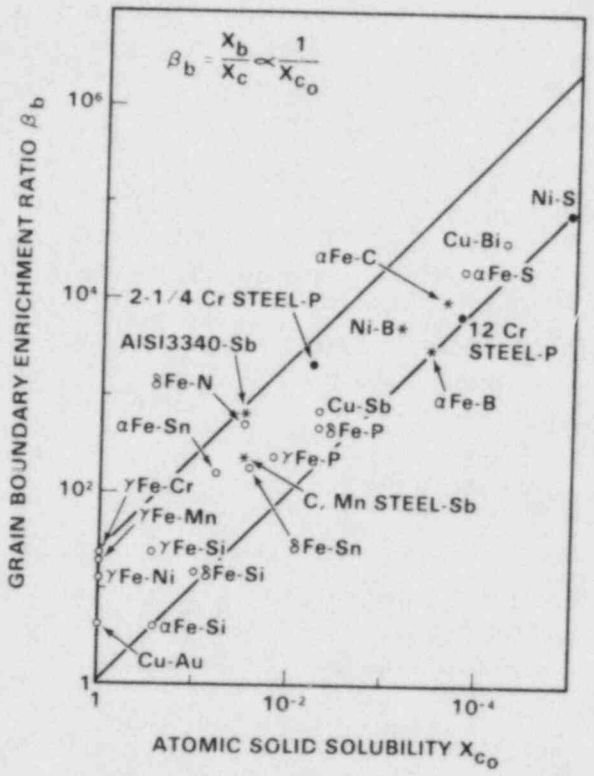

FIGURE 3.5. Correlation Between Measured Grain-Boundary Enrichment Ratios (β) and Inverse of Solid Solubility[72]

Type 304 SS alloy with 230 atomic ppm phosphorus. The temperature dependence of segregation is shown in Figure 3.6a and the segregation kinetics at 500°C in 3.6b.

Phosphorus has been shown by many investigators to promote intergranular corrosion in highly oxidizing solutions.[61-63,67-69] However, in high-temperature water environments most studies have indicated little or no effect of increasing bulk phosphorus concentration on IGSCC susceptibility. One exception is the work of Okada et al.,[73] which demonstrated the effect of phosphorus (and perhaps sulfur) when bulk carbon levels were less than 0.002%. At higher carbon levels, phosphorus additions did not reduce the strain necessary to produce IGSCC (in 300°C oxygenated water). A limitation of most of these results is that no direct measurement of segregation has been performed to document that increased bulk phosphorus levels increase the grain boundary composition of phosphorus.

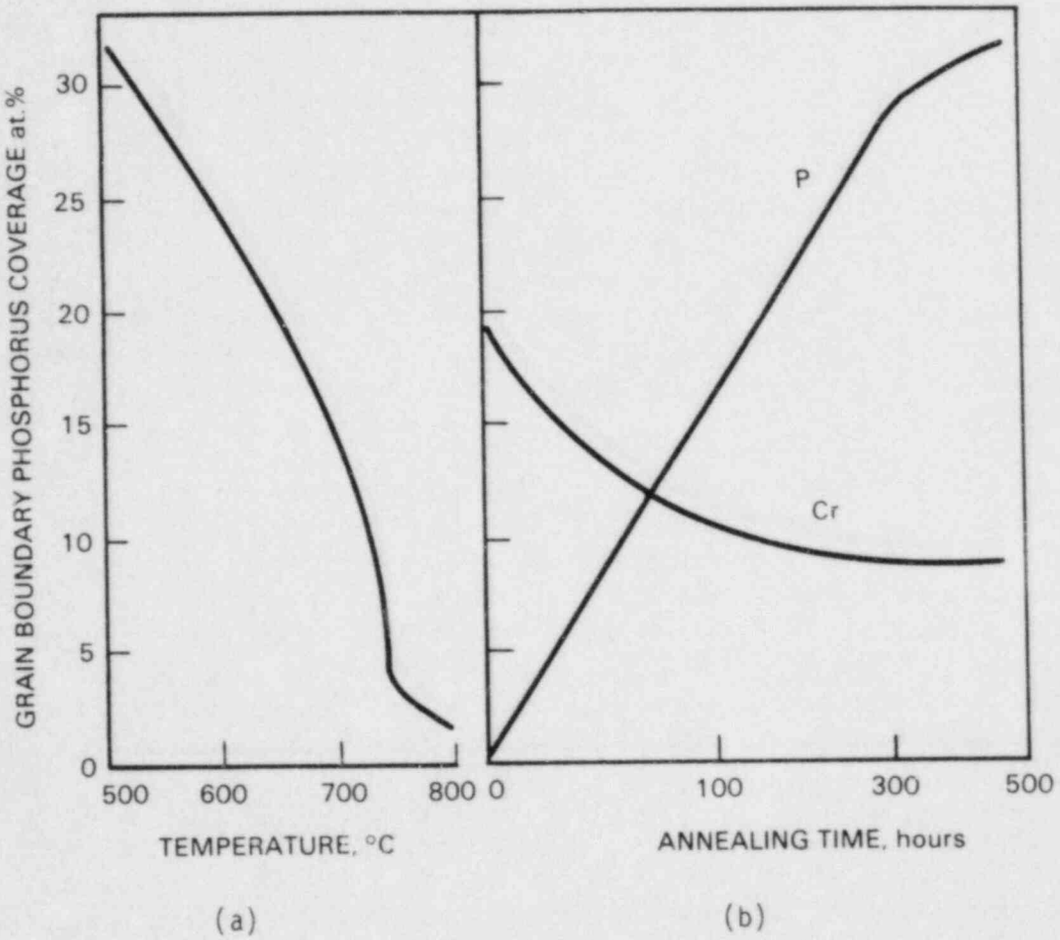

FIGURE 3.6. Auger Electron Spectroscopy Results of Lumsden and Stocker for Grain Boundary Segregation of Phosphorus in Type 304 SS: (a) Equilibrium Coverages and (b) Segregation Kinetics at 500°C

Another impurity commonly considered to be detrimental to corrosion and SCC resistance is sulfur. Sulfur has the potential to enrich grain boundaries at a factor of ~10^5 times the composition in solution. This concept is critical because most of the sulfur is tied up by reaction with manganese to form intragranular sulfides. Thus, the amount left in solution that is able to segregate is very small and, as a result, sulfur segregation is not often observed in steels. Corrosion and SCC tests on stainless steels with variable sulfur bulk concentrations do not show a strong effect of sulfur.[70,78] Perhaps, however, sulfur enrichment at interfaces is not great enough to be a factor. Sulfur has been observed to segregate rapidly to grain boundaries when the material is exposed to temperatures high enough (≥1200°C) to dissolve intragranular sulfides.[74] It is possible that such temperatures may be reached in HAZ regions close to the fusion line.

The effect of boron on intergranular corrosion has also been studied extensively, but often with contradictory results.[75-79] The most recent data by Robinson and Scurr[75] show a marked improvement in corrosion resistance with an addition of 4 ppm boron, which is believed to retard the precipitation of chromium-rich carbides, much as does nitrogen in the model proposed by Briant et al.[27] Other investigators have reported that boron can either improve resistance[76,77] or promote corrosion,[78,79] depending on heat treatment conditions and bulk boron concentration. Boron does segregate to grain boundaries as a result of both equilibrium[80] and nonequilibrium (vacancy drag during cooling)[81,82] processes. From the data available, it appears that boron equilibrium segregation reduces sensitization and corrosion susceptibility.

Silicon and nitrogen have also been observed to segregate to interfaces in austenitic stainless steels.[63,83] Since multiple impurity and alloying elements simultaneously enrich grain boundaries, an understanding of the interactions between these elements is critical for estimating the effect of individual elements. Competition between sulfur and phosphorus,[84] sulfur and nitrogen,[85] and phosphorus and carbon[86] has been observed in iron-based alloys. To what degree such competitions occur in austenitic stainless steels (and what effect they have on susceptibility) is not known at this time.

Several other elements may also improve or degrade the corrosion and/or SCC resistance of austenitic stainless steels. Sedriks[87] has assessed the relative effects of a large number of elements, as shown by the solid symbols in Figure 3.7. The majority of these correlations have been determined from tests of boiling magnesium chloride. This test environment is quite aggressive and promotes transgranular SCC. Alloying elements that are detrimental to chloride SCC resistance also tend to increase dislocation planarity by a reduction in the stacking fault energy or in short-range order.[88] Thus, these results are not directly applicable to IGSCC in high-temperature water environments.

Individual element effects on IGSCC in BWR environments have also been estimated and listed in Figure 3.7. The comparatively small number of elements indicated reflects the lack of systematic studies on compositional effects. Many of the relative effects listed have been estimated from properties of these elements in other alloys. For example, hydrogen recombinant poisons such as tin, antimony, and arsenic are detrimental due to their potential effect on hydrogen embrittlement.

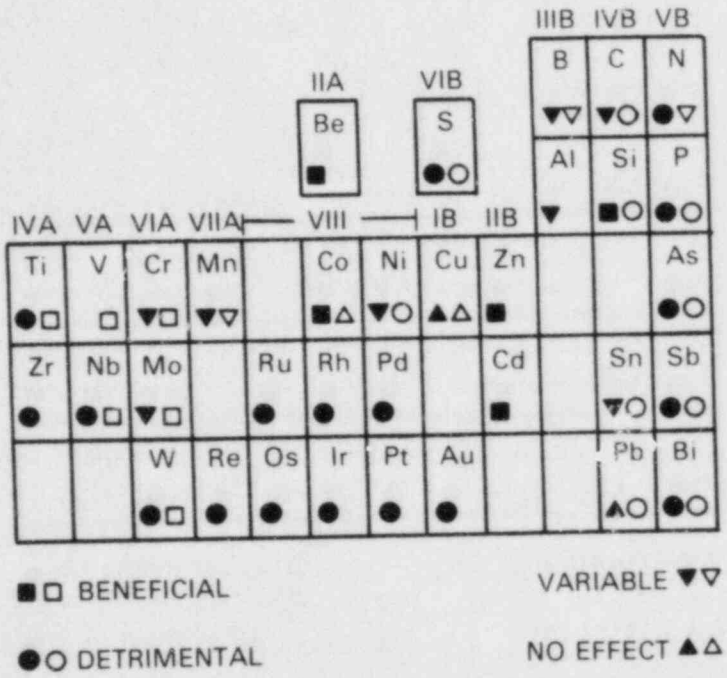

FIGURE 3.7. Effect of Various Alloying and Impurity Elements on the Resistance of Austenitic Stainless Steel to IGSCC in Chloride Solutions (solid symbols)[87] and High-Temperature Water Environments (open symbols)

3.4 NUCLEAR GRADE TYPES 304 AND 316 STAINLESS STEELS

The predominant effect of bulk carbon content on sensitization and IGSCC susceptibility has led to the development of two alternate stainless steel pipe materials.[89] These pipe materials have been designated as nuclear grade (NG) Types 304 and 316 stainless steels. The increased usage of these materials (particularly Type 316 NG) in nuclear power plant piping systems as either replacement or original piping has prompted considerable interest in their metallurgy and SCC resistance. Several aspects of the data base available on these materials will therefore be reviewed.

Nuclear grade materials are far more resistant to sensitization than standard grades because their carbon contents are limited to a maximum of 0.02 wt%. At these carbon levels, it is unlikely that typical welding practice will induce any significant sensitization in the HAZ. Laboratory and 4-inch and 16-inch pipe tests indicated that welded Types 304 NG and 316 NG were quite resistant to IGSCC in a BWR water environment.[44,89] However, it is important to note that

the NG steels are not immune to sensitization. Heat treatments (e.g., for stress relief) at temperatures in the sensitization range must still be avoided.

Although carbon has been shown to be the primary element controlling sensitization and IGSCC, other elements, particularly segregating impurities, also have a significant effect on cracking susceptibility. The reduction of carbon may increase the importance of elements such as phosphorus, sulfur, and silicon (see Section 3.3). Lower bulk carbon may also increase the potential for martensite formation by raising the M_s temperature (see Section 2.4). Thus, even though classical sensitization is avoided, a microstructure susceptible to SCC might be developed in the HAZ during welding.

Another concern in the use of the NG steels is the potential for transgranular (TG) SCC since the susceptibility to IGSCC has been reduced. The presence of higher levels of nitrogen (0.06 to 0.10 wt%) in stainless steels is known to increase TGSCC susceptibility, particularly in chloride environments. Recent work has shown that Type 316 NG is susceptible to TGSCC in slightly impure BWR water.[90] Preliminary results indicate that this cracking propagates at a sufficiently slow rate so that, even if initiated, it may not be a significant problem under service conditions. However, control of environment impurities remains important to ensure resistance to both IGSCC and TGSCC. A recent report by the U.S. NRC Piping Review Commission summarizes much of the available SCC test data on Type 316 NG.[91]

A final potential problem area is solidification cracking. There have been reports of cracking as a result of seam welding Type 316 NG under certain conditions. Solidification cracking in the weld metal depends on three main factors: 1) coarseness of the microstructure, 2) segregation, and 3) joint geometry. The most detrimental segregants are believed to be impurities such as sulfur and phosphorus. Both have been observed to be segregated on interfaces opened by solidification cracks.[92] Weld simulation (varestraint) tests indicated much higher susceptibility to cracking for Type 316L (and 316) than for Type 304 stainless steel.[93]

In summary, NG stainless steels are significantly more resistant to sensitization than standard grades. As a result, these materials exhibit good resistance to IGSCC in BWR water environments. The data base is insufficient at present to ensure immunity to cracking in service. Areas that require additional understanding include impurity segregation effects on IGSCC, environmental impurity effects on TGSCC, and solidification cracking resistance.

4.0 METHODS TO PREDICT MATERIAL SENSITIZATION

4.1 COMPOSITION-BASED MODELS

The effect of alloying and impurity elements on sensitization and IGSCC susceptibility was discussed in Section 3. The purpose of this review is not only to obtain a qualitative understanding of individual element potencies, but to assess methods to predict a particular alloy's sensitization propensity from its bulk composition. Idea ly, a predictive model should be based on 1) the effect of each element on the local chromium depletion and 2) any direct effect an element may have on the local dissolution/passivation characteristics when enriched or depleted at grain boundaries. Unfortunately, this type of information is not available in a form that can be used quantitatively. As a result, models that most effectively predict composition effects have been empirically based through correlation to intergranular corrosion and SCC susceptibility data.

Cihal[59] rationalized heat-to-heat variability in intergranular corrosion and SCC resistance by normalizing compositional differences with "effective" chromium and carbon concentrations. Chromium concentration was normalized in relation to molybdenum, and carbon was normalized in relation to nickel:

$$Cr_{eff} = Cr + k_1\ Mo \tag{11}$$

$$C_{eff} = C + k_2\ [Ni - k_3] \tag{12}$$

The concentrations of each element were expressed as weight percentages, and the constants were defined by Cihal as k_1 = 1.0 to 1.7, k_2 = 0.002, and k_3 = 10. Equivalent SCC resistance was suggested for alloys with equal values of

$$K = Cr_{eff} - 100\ C_{eff} \tag{13}$$

This equivalency concept is shown graphically in Figure 4.1, where heat compositions along one of the solid lines indicate equivalent IGSCC resistance. The solid lines were extrapolated from the points shown representing typical Type 304 (18.5 Cr, 8.5 Ni, 0.2 Mo, 0.05 C) and 316 (17.0 Cr, 12.5 Ni, 2.2 Mo, 0.05 C) stainless steel compositions. Increased susceptibility (over the typical alloys) is predicted for alloys that lie to the right of these lines and decreased susceptibility for those to the left. Commercial alloy compositions can fall anywhere within the dashed lines, producing a wide variation in potential susceptibility due to changes in bulk composition.

The equivalent SCC resistance term, K, enables the assessment and ranking of individual heats. Higher values of K suggest improved SCC resistance. Since the primary cause of sensitization and IGSCC is chromium depletion, this

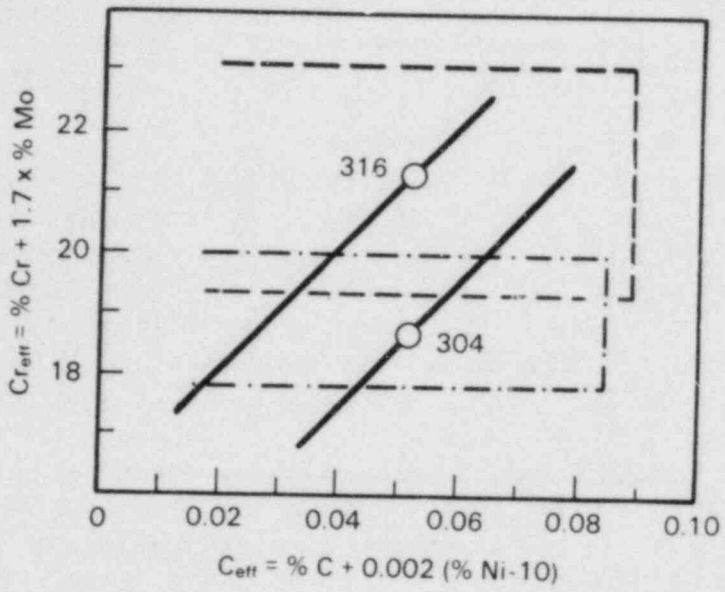

FIGURE 4.1. Intergranular SCC Equivalency Plot Using the Empirically Derived Parameters of Cihal.[59] Solid lines are IGSCC equivalency lines that were drawn by extrapolation from typical Type 304 and 316 SS compositions.

term also indicates the potential chromium levels at grain boundary regions. Therefore, redefining K as a "composite" chromium value (Cr*) improves the physical meaning of this term since its magnitude can be tied directly to the phenomenon. Combining Equations 11 through 13 and entering the appropriate constants will allow the determination of composite chromium values by:

$$Cr^* = Cr + (1.0 \text{ to } 1.7)\ Mo - 100\ C - 0.2\ Ni + 2 \qquad (14)$$

The effect of bulk carbon (the most important element in sensitization propensity, as discussed in Section 3.1) on Cr* values is illustrated in Figure 4.2, where Cr* ranges from ~19% for low-carbon Type 316L down to ~11% for high-carbon Type 304 SS.

The concept that the Cihal parameters must be related to local chromium concentrations prompted Fullman[11] to compare thermodynamically derived chromium equivalency parameters to those of Cihal for selected alloying elements. The basis for these calculations assumed that an alloy's susceptibility to IGSCC could be judged by the chromium concentration in equilibrium with a $M_{23}C_6$-type carbide. Individual alloying elements were then assessed by considering their effect on several factors including carbide formation and carbon activity, and ultimately, the equilibrium chromium concentration adjacent to the carbide. The resultant chromium-equivalency parameters (listed in Table 4.1) represent the change in alloy chromium concentration for a 1%

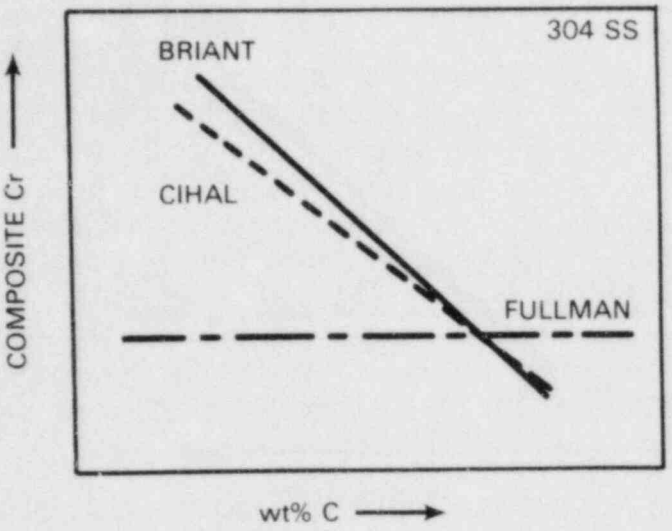

FIGURE 4.2. Composite Chromium Values Calculated Using the Parameters of Cihal[59], Fullman,[11] and Briant[27] as a Function of Bulk Carbon Content

TABLE 4.1. Chromium-Equivalency Parameters of Fullman[11]

Element	Fe-Ni-Cr Thermodynamics		Empirical Values,
	Kaufman and Nesor[94]	Hasebe and Nishizawa[95]	Cihal[59]
C	-157 at 0.03% C	-161 at 0.03%C	-100
	-118 at 0.04% C	-121 at 0.04%C	
	-94 at 0.05% C	-97 at 0.05%C	
	-79 at 0.06% C	-81 at 0.06%C	
	-67 at 0.07% C	-69 at 0.07%C	
Log C	-10.85	-11.14	
Ni	-0.01	-0.19	-0.2
Mo	1.45	1.45	1.0 to 1.7
Al	-0.40 to 0.04	-0.51 to 0.14	
Co	-0.14	-0.20	
Cu	0.06	0.01	
Mn	0.17	0.13	
Si	-0.11 to 0.32	-0.22 to 0.23	
Ti	0.75 to 1.48	0.61 to 1.45	
V	0.43 to 1.00	0.34 to 0.98	
W	0.23	0.22	

addition of the particular alloying element. Thus, these parameters can be compared directly to those of Cihal as shown in Table 4.1.

The relative magnitude and sign of the thermodynamically based parameters of Fullman and the empirically based parameters of Cihal are quite good.

However, the carbon parameter changes as a function of carbon concentration and, as a result, does not predict increasing susceptibility with increasing bulk carbon. Composite chromium values calculated using these parameters are nearly independent of carbon concentration, as shown in Figure 4.2. This could be the case if the strong dependence of sensitization and IGSCC susceptibility on carbon level results from $M_{23}C_6$ precipitation kinetics, not thermodynamics. Thus, decreasing bulk carbon levels delay the nucleation and limit the number of $M_{23}C_6$ carbides, but do not significantly change the local chromium concentration in equilibrium with the carbide once it is nucleated. However, this is not consistent with predictions of Stawstrom and Hillert[2] or Tedmon et al.[3]

Calculations of equilibrium chromium concentration as a function of carbon content have been performed by both Stawstrom and Hillert and Tedmon et al. as shown in Figure 4.3. Increasing carbon content can be seen to sharply decrease chromium content at relevant temperatures. Therefore, the carbon equivalency parameter terms listed by Fullman[11] are in sharp contrast to predictions from both empirical and thermodynamic models.

Fullman's initial parameter for molybdenum was small (~0.35) when based solely on thermodynamic data for a $Mo_{23}C_6$ carbide. To achieve the parameter listed in Table 4.1, the combined concentration of chromium and molybdenum adjacent to the carbide was determined. This combined element calculation was justified because of the effect of molybdenum on the passivation of austenitic stainless steel (see Section 3.2). The local depletion of molybdenum has been shown to contribute to an alloy's susceptibility to intergranular corrosion.[27]

A significant benefit from Fullman's thermodynamic calculations is the generation of chromium-equivalency parameters for many additional elements present in stainless steels. Most of the elements have a very small effect on the calculated value of Cr* unless there is a significant change in their normal compositions. In order to use these parameters to calculate Cr* and compare it to sensitization data, the Cihal parameter for carbon will be substituted for Fullman's values, following Briant et al.,[27] and the lower values for the Al, Si, Ti, and V parameters (calculated using the estimated lower limit for the standard free energy of formation of non-occurring $M_{23}C_6$ carbides) will be used to give:

$$Cr^* = Cr + 1.45\,Mo - 0.19\,Ni - 100\,C - 0.51\,Al - 0.2\,Co + 0.01\,Cu + 0.13\,Mn - 0.22\,Si + 0.61\,Ti + 0.34\,V + 0.22\,W \quad (15)$$

Even though the Fullman parameters indicate relative effects of many alloying elements, it would be particularly useful to also consider the effects of more important elements, such as nitrogen, phosphorus, and boron. Clark et al.[66] recently used time/temperature/sensitization data to determine the

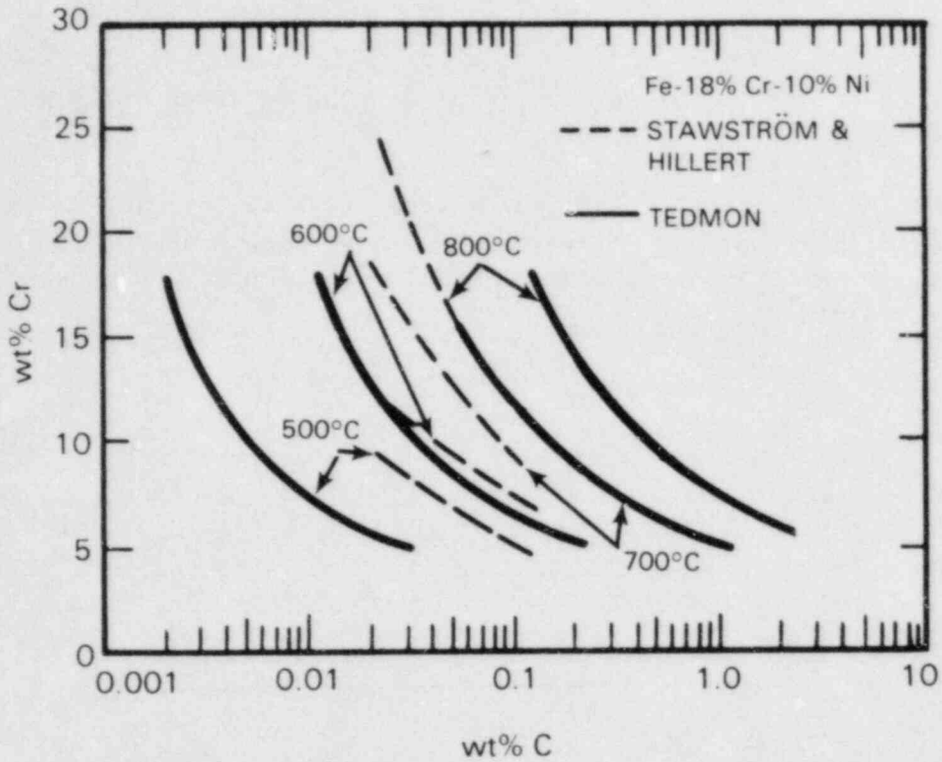

FIGURE 4.3. Cr-C-$Cr_{23}C_6$ Equilibrium Data for Type 304 SS Predicted Using Methods of Stawström and Hillert[2] and Tedmon et al.[3]

effect of nitrogen on the chromium concentration in equilibrium with $M_{23}C_6$ carbides. These calculations were made by assuming that nitrogen retards sensitization (as discussed in Section 3.2) by increasing the local chromium concentration. Their data, along with that of Briant et al.[27] and Binder et al.,[38] can be used to estimate the chromium equivalency parameter for nitrogen. Examination of data suggests that each increase of 0.01 wt% nitrogen increases the local chromium content (and Cr*) by ~0.092 wt%; therefore, a nitrogen term of +9.2 N could be added to Equations 14 and 15. It is probable that this type of empirical factor could be developed for other elements as well, but the data base is simply too limited.

Although this review is not specifically concerned with the stabilized grades of austenitic stainless steel, it is important to note that correlations have been developed to account for the effect of stabilizing element addition on intergranular corrosion and SCC resistance.[29] The approach has been to determine from the concentration of stabilizing element addition the amount of carbon that would be precipitated into nonsensitizing carbides and therefore not available for sensitizing carbide ($M_{23}C_6$) formation. An example of such a relationship for titanium is:

$$C_{TiC} = f \frac{Ti - 3.43\ (N - 0.001)}{4} \qquad (16)$$

where f = 1 after a stabilizing heat treatment and N is the bulk nitrogen concentration.

Another material factor that is critical to sensitization development and SCC susceptibility is grain size. Attempts have been made[29] to modify the equivalent SCC resistance equation of Cihal (Equation 13) to account for changes in grain size:

$$K = Cr_{eff} - 100\ C_{eff}/1.2\ \sqrt{2^{N-1}} \qquad (17)$$

where N is the ASTM grain size number. An example of the effect of grain size on an IGSCC equivalency plot is shown in Figure 4.4. As expected, increasing grain size increases susceptibility to corrosion. While grain size does have a significant effect on sensitization, the data available are insufficient to determine whether the simple correlation in Equation 17 and Figure 4.4 could be used quantitatively.

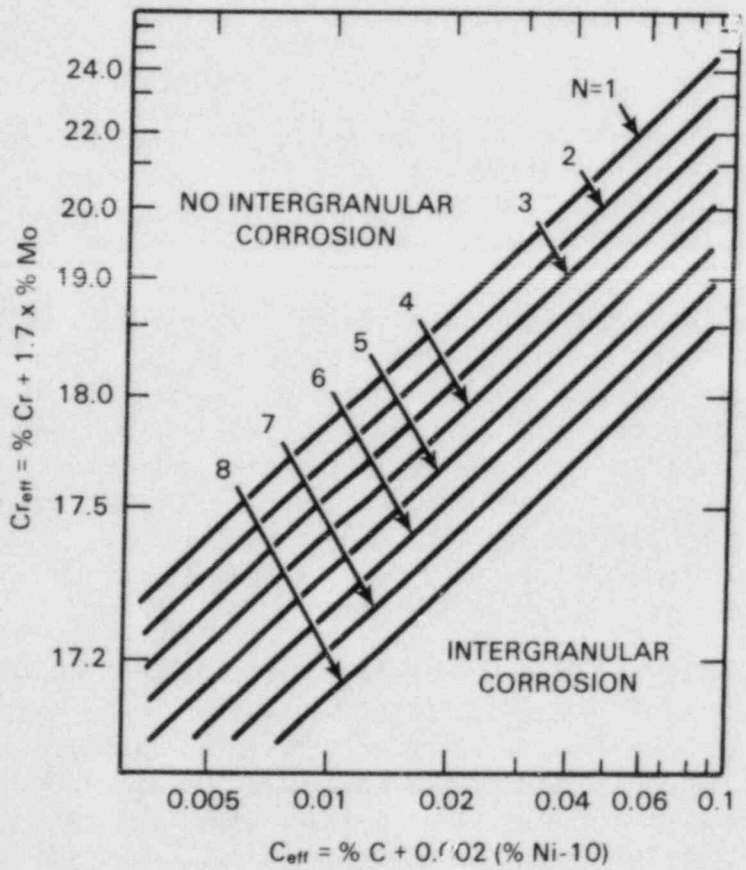

FIGURE 4.4. Grain Size Modified Cihal Parameter Plot. After Cihal.[29]

4.2 ASSESSMENT OF PREDICTIVE CAPABILITY

The sensitization and IGSCC potential of any heat of material is primarily controlled by its bulk composition. This fact is the basis for Cihal's[59] empirical formulation to rationalize compositional effects. Several proposed variations of this "standard" method were discussed in the previous section. In order to assess the predictive capability of these methods, a data base of time/temperature/sensitization curves from more than 100 heats of Types 304 and 316 SS has been compiled. Only DOS measurements from Strauss, modified Strauss, or EPR test techniques were compared (see Appendix A). The most consistent data for comparison purposes was measured times-to-sensitize as a function of heat treatment temperature.

The composition-based sensitization prediction equations evaluated are listed in Table 4.2. They range in complexity from a simple correlation to bulk carbon content (see Section 3.1) to the eleven elements in Fullman's model.[11] Linear regression analysis was performed using each of the formulations versus time-to-sensitize data at 600°C, 650°C, and 700°C. These temperatures were the only ones for which sufficient data existed to allow statistical comparisons. The relative "fit" of the particular model prediction to the data is also shown in Table 4.2 (the lower the variance, the better the fit). Considering the source of this data, the strong positive correlations (<0.4) recorded for several of the predictive equations are promising.

The addition of many other elements in the Fullman model only slightly modifies the composite chromium prediction and thus has no significant effect on predictive capability. Preliminary attempts were also made to include nitrogen in model predictions; however, no significant improvement was found even when considering nitrogen effects that were dependent on carbon and molybdenum concentrations. The best predictive capability was obtained using a slightly modified version of Cihal's parameters. Many of the equations in Table 4.2 result in predictions of comparable accuracy.

A typical correlation between prediction and the time-to-sensitize data base is shown graphically in Figure 4.5. This correlation enables "factors of improvement" based on time to sensitize to be calculated as a function of material bulk composition. A simple method to determine these factors (for heat-to-heat comparison purposes) is outlined in Appendix B.

It is important to note from Figure 4.5 that the scatter in experimental time-to-sensitize data for a particular Cr* can be as much as two orders of magnitude. This scatter is primarily due to variations in initial material condition (e.g., mill annealed, solution annealed, or cold worked), differences in experimental techniques among laboratories (e.g., test time or evaluation criteria to detect sensitization) and difficulties in accurately identifying the time to sensitize from the reported data. Thus, although the Cr* equations

TABLE 4.2. Correlation Between Predictions from Composition-Based Models to Time-to-Sensitize (t_s) Data Base

Predictive Equation Source	Formula for Composite Chromium, Cr*	Linear Regression Correlation Equation	Data "Fit" at 650°C, Variance
Carbon content	C	$\log t_s = 1.87 - 36.47\ C$	0.55
Cihal-1.0	Cr + 1.0 Mo - 0.2 Ni - 100 C	$\log t_s = -3.82 + 0.326\ Cr^*$	0.473
Cihal-1.3	Cr + 1.3 Mo - 0.2 Ni - 100 C	$\log t_s = -4.03 + 0.338\ Cr^*$	0.388
Cihal-1.5	Cr + 1.5 Mo - 0.2 Ni - 100 C	$\log t_s = -4.00 + 0.330\ Cr^*$	0.350
Cihal-1.6	Cr + 1.6 Mo - 0.2 Ni - 100 C	$\log t_s = -3.96 + 0.325\ Cr^*$	0.341
Cihal-1.7	Cr + 1.7 Mo - 0.2 Ni - 100 C	$\log t_s = -3.96 + 0.324\ Cr^*$	0.347
Briant	Cr + 1.42 Mo - 0.18 Ni - 100 C	$\log t_s = -4.11 + 0.335\ Cr^*$	0.374
Fullman	Cr - 1.45 Mo - 0.19 Ni - 100 C + 0.13 Mn - 0.22 Si - 0.51 Al - 0.20 Co + 0.01 Cu + 0.61 Ti + 0.34 V - 0.22 W	$\log t_s = -4.07 + 0.332\ Cr^*$	0.364
Nitrogen modified	Cr - 1.6. Mo - 0.2 Ni - 100 C + 9.2 N	$\log t_s = -3.89 + 0.310\ Cr^*$	0.365
Carbon modified	Cr + 1.6 Mo - 0.2 Ni - 110 C	$\log t_s = -3.50 + 0.300\ Cr^*$	0.385
Mn/Si modified	Cr + 1.6 Mo - 0.2 Ni - 100 C + 0.13 Mn - 0.22 Si	$\log t_s = -4.02 + 0.328\ Cr^*$	0.349
Ni modified	Cr + 1.6 Mo - 0.18 Ni - 100 C	$\log t_s = -4.03 + 0.325\ Cr^*$	0.356
Ni modified	Cr + 1.6 Mo - 0.22 Ni - 100 C	$\log t_s = -3.93 + 0.328\ Cr^*$	0.365

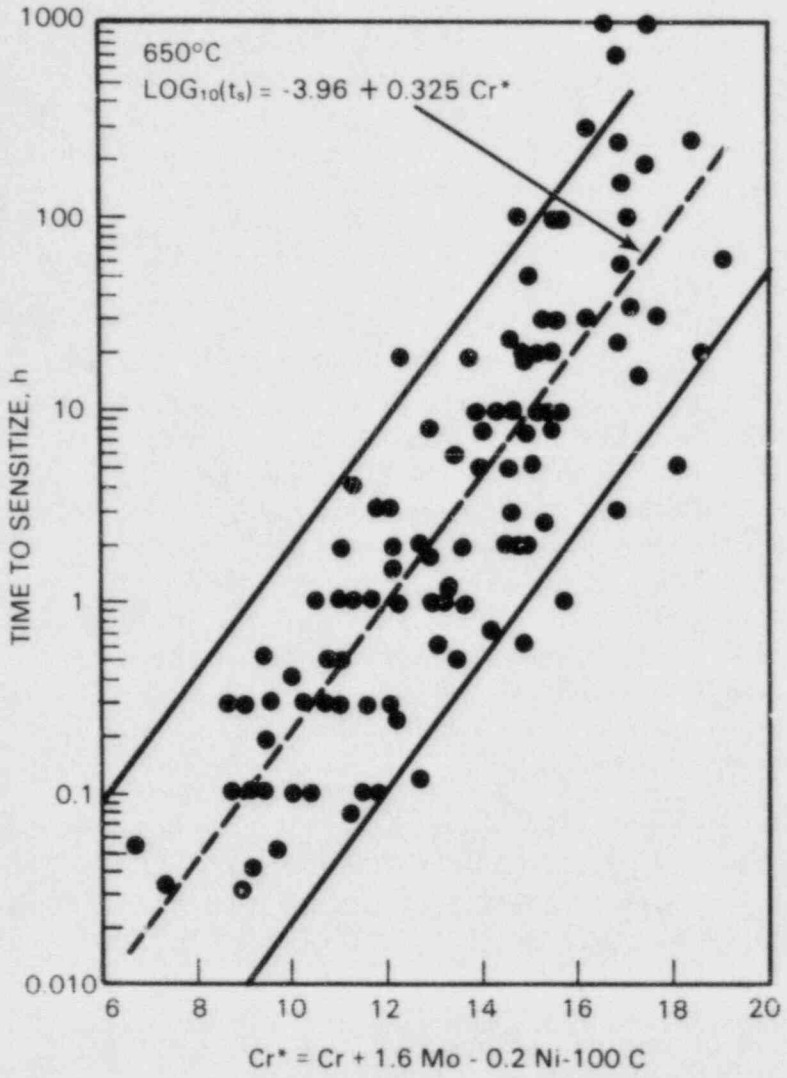

FIGURE 4.5. Correlation Between Composition Normalization Parameter, Cr*, and Experimentally Measured Time-to-Sensitize Data

fit the trend of the isothermal sensitization data, they cannot be used to quantitatively predict sensitization times.

4.3 CHROMIUM DEPLETION MODEL

The previous sections have approached sensitization prediction solely from a compositional point of view. This approach only allows the prediction of a materials sensitization potential. Sensitization development and therefore the prediction of actual DOS as a function of thermal history depends on the kinetics of chromium and carbon diffusion. The precipitation of $M_{23}C_6$ carbides requires the transport of chromium and carbon by diffusion to grain boundaries. As shown in Section 2.1, the diffusion of carbon in austenitic steels is about

4 orders of magnitude greater than that of chromium, so that a chromium-depleted zone will develop near the precipitating carbide. When the chromium concentration near the grain boundary falls below some critical value, estimated at 13 to 15 wt%, passivity will be affected, and the alloy will become susceptible to intergranular attack.

Bain, Aborn, and Rutherford[1] developed a model explaining intergranular corrosion that attributes sensitization to the precipitation/depletion process. Stawström and Hillert[2] later described a method for calculating the chromium concentration near the grain boundary, the time to sensitize, and the depleted width. Tedmon et al.[3] used the same basic assumption in the Cr depletion model (i.e., the chromium concentration at the grain boundary determines sensitization and is thermodynamically fixed). Unlike Stawström and Hillert, Tedmon et al. assumed that there could be a chromium gradient between carbide particles as well as a gradient normal to the grain boundary. (The Tedmon diffusion analysis did show that chromium depletion may be nearly uniform despite a wide separation of carbide particles.) Tedmon et al. further suggested that the thermodynamic analysis is amenable to estimating the effect of alloy composition on the chromium concentration (and subsequent sensitization), showing that DOS is strongly affected by a thermodynamic minimum chromium content and less affected by carbide morphology.

In applying the chromium depletion theory to experimental data, most comparisons are made to the Stawström and Hillert model.[2] The following is a summary of the expressions generally used to estimate chromium depletion parameters. The reader is referred to the original references for the development of these equations.

- Total width of the Cr-depleted zone, ℓ:

$$\ell \cong 2\sqrt{2Dt} \tag{18}$$

where D is the Cr diffusivity and t is the time at temperature.

- Width of the Cr-depleted zone where the Cr content is less than that required for passivation, m:

$$m = 2\sqrt{Dt}\left(\frac{x^{C}_{Cr} - x^{i}_{Cr}}{x^{o}_{Cr} - x^{i}_{Cr}}\right) \tag{19}$$

where X^c_{Cr} = critical Cr content required for passivation,

X^i_{Cr} = Cr content at the carbide interface established by the thermodynamics of the carbide-matrix system, and

X^o_{Cr} = bulk alloy Cr concentration.

- Time for self-healing (desensitization), t_{SH}:

$$t_{SH} = \left(\frac{h\, X^o_C}{X^o_{Cr} - X^C_{Cr}} \right)^2 / D \qquad (20)$$

where h = average grain diameter and X^o_C = bulk carbon content.

Numerous investigators have used the Stawström and Hillert formulations to predict sensitization development. The success of these predictions has been somewhat mixed, but, on the whole, quite promising. It is obvious that the correct process--i.e., chromium diffusion--is being modeled. However, in most cases, very little parameter optimization has been attempted to improve prediction capability. One critical parameter that needs accurate definition is the local chromium concentration adjacent to $M_{23}C_6$ carbide. Direct measurement techniques such as Auger electron spectroscopy and analytical electron microscopy can be used to document this concentration as a function of heat treatment temperature and material bulk composition. Examples of these measurements are given in Appendix A.

At the present time, composition-based equations can be used to estimate the sensitization potential of any heat. It is our contention that this composite chromium term is directly related to the local chromium concentration and can be normalized for use with a Stawström and Hillert-type kinetic analysis. This combination enables the prediction of actual DOS values as a function of thermal treatment. Such an analysis will be applicable only for treatment within or through the rapid sensitization temperature range. The flow diagram in Figure 4.6 illustrates the steps necessary for this type of prediction methodology.

4.4 APPLICABILITY OF MODELS TO WELD HEAT-AFFECTED ZONE SENSITIZATION

This review of compositional effects on sensitization has been limited to isothermal data comparisons, because there is a large isothermal data base of DOS measurements as a function of material composition. Unfortunately, no comparable data base exists for weld sensitization. The previous section discussed the methodology of DOS prediction; this section describes the requirements and modifications necessary for weld HAZ DOS prediction.

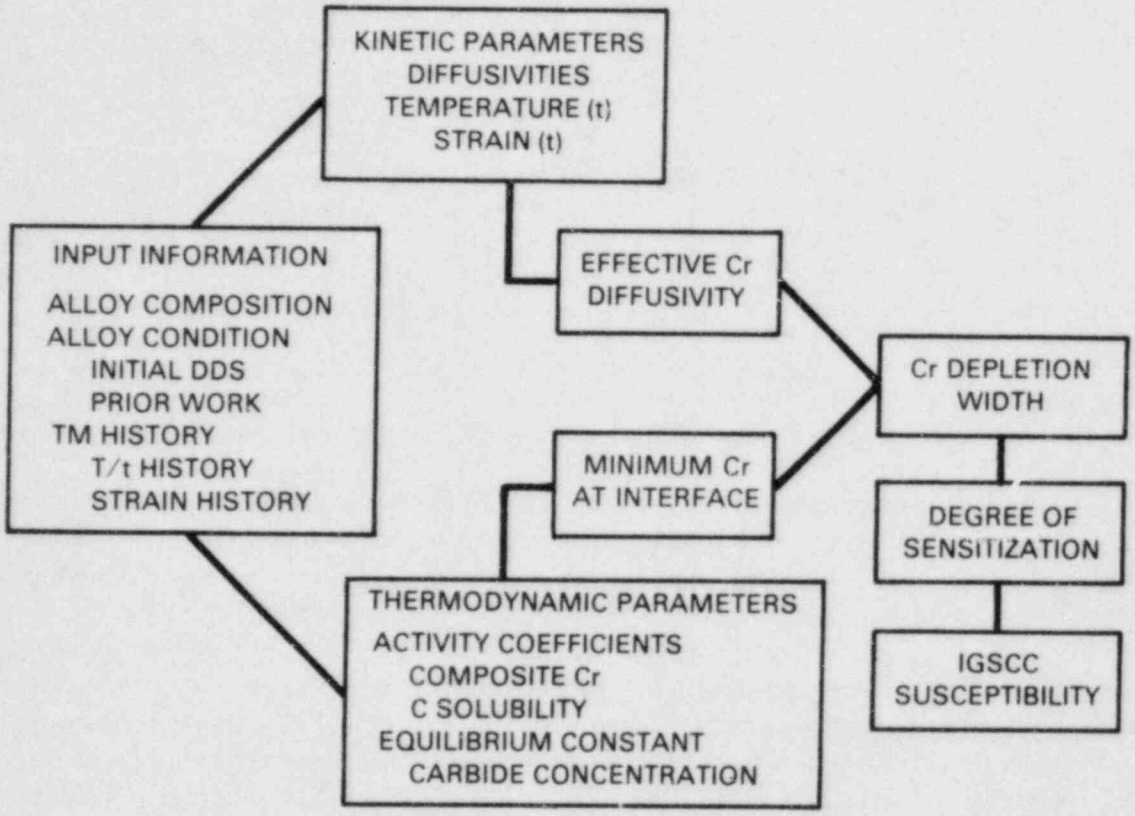

FIGURE 4.6. Methodology for Prediction of the Degree of Sensitization and IGSCC Susceptibility as a Function of Material Composition and Thermal Treatment

The development of sensitization within a HAZ involves more than a simple isothermal heat treatment. Sensitization depends on the weld heat input, interpass temperature, pipe size, and other variables. An example of an "idealized" weld HAZ thermal cycle is shown in Figure 4.7. Two aspects of these cycles are critical for sensitization development: peak temperature and cooling rate.[96] Summation methods have been devised to directly input this type of temperature/time data into a kinetics model based on chromium diffusion (as discussed in Section 4.3). However, there are insufficient DOS data at this time to evaluate the ability to predict DOS after thermal cycling.

Composition effects on sensitization during continuous cooling appear to be comparable to those predicted from isothermal data. Solomon[97] has documented the dominant influence of bulk carbon content on the peak temperature for maximum sensitization during continuous cooling and on the critical cooling rate required for sensitization (Figure 4.8). The correlation shown in Figure 4.8 corresponds to the effect of carbon on the time required for sensitization during isothermal heat treatment (shown in Figure 3.2). Nitrogen was also

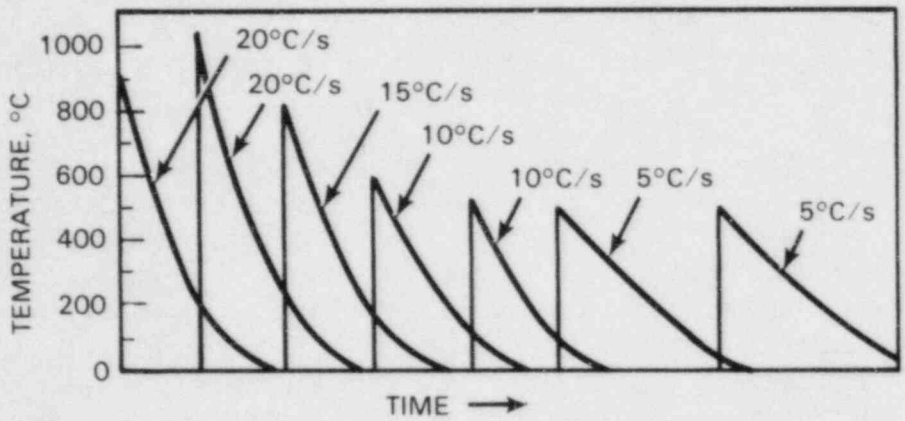

FIGURE 4.7. Schematic Illustrating Weld HAZ Thermal Cycles(97)

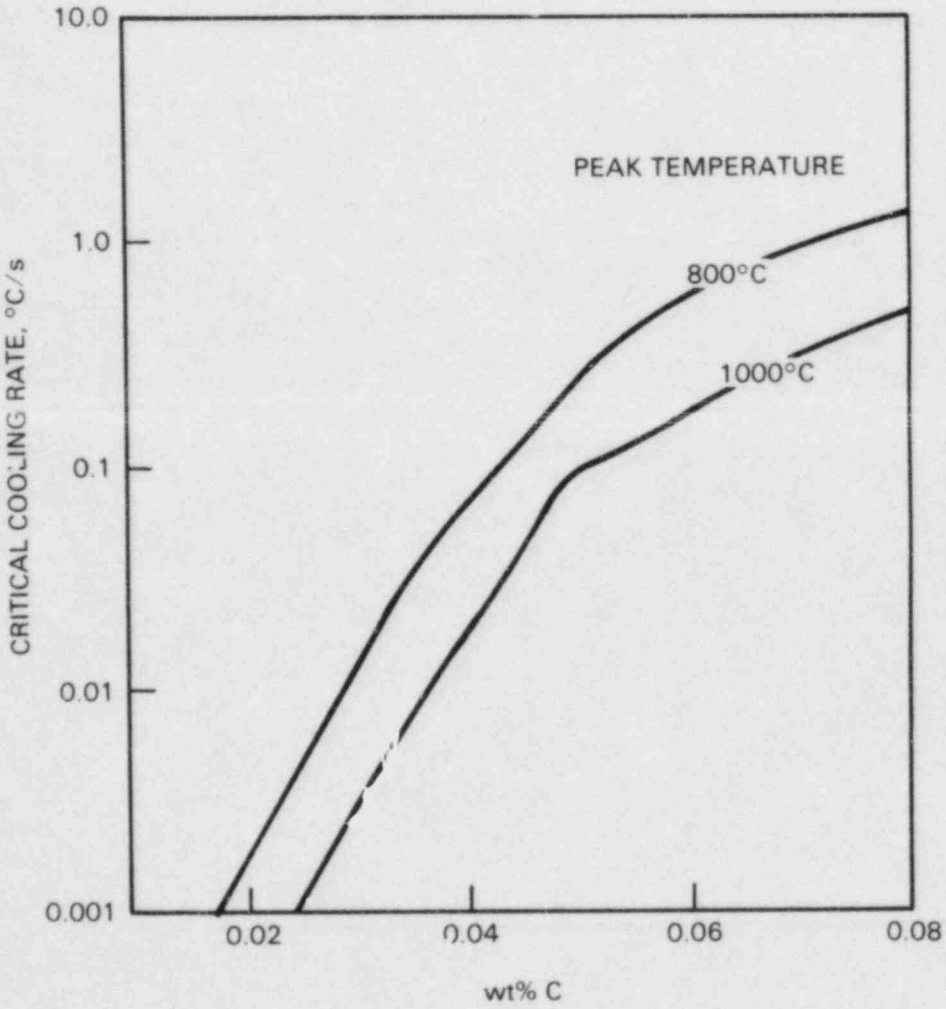

FIGURE 4.8. Critical Cooling Rate for Sensitization as a Function of Bulk Carbon Content(97)

found to produce an improvement in sensitization resistance similar to that discussed for isothermal data in Section 3.2. These results indicate that the composition-based models derived from isothermal data are applicable to the complex thermal cycling situation in a weld HAZ.

Perhaps the most critical aspect of HAZ sensitization is the presence of simultaneous deformation. It is certainly the most difficult to predict. Plastic strain has been shown to exacerbate sensitization development by significantly decreasing the time to sensitize. A logical approach to modeling the effect of strain on sensitization development is to modify chromium and carbon diffusivities as a function of strain. It is impossible, with the data available, to assess the potential of such an approach. However, as the data base grows, empirically based parameters in the diffusivity equations can be determined. Therefore, a methodology can be prepared that adds on to the basic approach (Figure 4.6) and enables the prediction of HAZ DOS on a pass-by-pass basis.

5.0 CONCLUSIONS

The effects of alloying and impurity elements on the sensitization propensity of Types 304 and 316 stainless steel have been reviewed. As expected, carbon was found to be the dominant element controlling sensitization, with chromium, molybdenum, and nickel also important. Other alloying elements, such as manganese and silicon, have at most only a small effect on sensitization. However, strongly segregating elements, such as nitrogen, boron, and phosphorus may have a significant effect on intergranular corrosion and SCC susceptibility.

Composition-based models to predict sensitization propensity were assessed. Chromium-equivalency parameters were used to calculate a normalized term (composite chromium) that is related to the equilibrium chromium concentration in austenite adjacent to a $M_{23}C_6$ carbide. Composite chromium values were observed to effectively normalize compositional variations by comparison with time-to-sensitize data from more than 100 time/temperature/sensitization curves. A combination of this type of composition-based model with a kinetics model based on chromium diffusivity appears to be applicable to at least semi-quantitative DOS predictions. A methodology is proposed by which DOS can be estimated from material composition and thermomechanical history information.

6.0 REFERENCES

1. E. C. Bain and R. H. Aborn, Trans. Am. Soc. Steel Treat., Vol, 18, 1930, p. 837.

2. C. Stawstrom and M. Hillert, J. Iron and Steel Inst. January 1969, p. 77.

3. C. S. Tedmon, Jr., D. A. Vermilyea and J. H. Rosolowski, J. Electrochem. Soc., Vol, 118, 1971, p. 1971.

4. T. M. Devine, J. Electrochem. Soc., Vol, 126, 1979, p. 374.

5. R. L. Cowan and G. M. Gordon, Proc. Conf. Stress Corr. Cracking and Hydrogen Embrittlement, NACE, Houston, 1977, p. 1025.

6. K. Osozawa and H. J. Engell, Corr. Soc., Vol. 6, 1966, p. 589.

7. K. Arioka, M. Hourai, S. Nocuchi and K. Onimura, Corrosion/83, Paper No. 134, April 1983.

8. R. B. Snyder, K. Natesan and T. F. Kassner, Report ANL-8015, Argonne Natl. Lab., June 1973.

9. R. Stickler and A. Vinckier, Trans. ASM., Vol. 54, 1961. p. 362.

10. K. Natesan and T. F. Kassner, Nuc. Tech., Vol. 19, 1973. p. 46.

11. R. L. Fullman, Acta Met, Vol. 30, 1982, p. 1407.

12. H. E. Hänninen, Inc. Metals Rev., No. 3, 1979, p. 85.

13. T. M. Devine, Trans. ASM., Vol. 11A, 1980. p. 791.

14. B. Weiss and R. Stickler, Met. Trans., Vol. 3, 1972. p. 851.

15. V. Cihal and I. Kasova, Corr. Sci., Vol. 10, 1969. p. 875.

16. J. K. L. Lai, Mat Sci. & Eng., Vol. 61, 1983. p. 101

17. G. H. Eichelman and F. C. Hull, Trans ASM, Vol. 45, 1953, p. 77.

18. F. C. Monkman, F. G. Cuff and N. Grant, Metal. Prog., Vol. 71, 1957, p. 71.

19. E. W. Collings and H. W. King, in the Metal Science of Stainless Steels, ed. E. W. Colling and H. W. King, TMS-AIME, 1978, p. 1.

20. E. P. Butler and M. G. Burke, Proc. of Int. Conf. on Solid-Solid Phase Transformations, ed. H. I. Aaronson, D. E. Laughlin, R. F. Sekarka and C. M. Wayman, TMS-AIME, 1981, p. 775.

21. M. G. Lackey and F. J. Humphreys, Proc. 3rd Intern. Conf. on Effects of Hydrogen on Behavior of Materials, ed. I. M. Bernstein and A. W. Thompson, TMS-AIME, Warrendale, PA, 1980, p. 665.

22. C. L. Briant and A. M. Ritter, Metall. Trans., Vol. 11A, 1980, p. 2009.

23. P. K. De, G. C. Paht and K. Elayaperumal, Trans. Ind. Inst. Metals, Vol. 26, 1973, p. 56.

24. A. Randak and F. W. Trantes, Werks. and Korros., Vol. 21, 1970, p. 97.

25. C. L. Briant, Metall. Trans., Vol. 9A, 1978, p. 731.

26. D. G. Atteridge, S. M. Bruemmer and R. E. Page, NUREG/CR-3613, Annual Report, 1983, p. 33.

27. C. L. Briant, R. A. Mulford & E. L. Hall, Corrosion, Vol. 38, No. 9, 1982, p. 468.

28. R. A. Mulford, E. L. Hall & C. L. Briant, Corrosion, Vol. 39, No. 4, 1983, p. 132.

29. V. Cihal, Protection of Materials (Zashcita Metallur.), Vol. 4, No. 6, p. 563.

30. M. J. Povich, Corrosion, Vol. 34, No. 2, 1978, p. 60.

31. H. D. Solomon, Corrosion, Vol. 36, No. 7, 1980, p. 356.

32. F. Umemura & T. Kawamoto, in Predictive Methods for Assessing Corrosion Damage to BWR Piping and PWR Steam Generators, ed. H. Okada and R. Staehle, NACE 1982, p. 209.

33. Eckenrod & Kovach, ASTM STP 679, 1979, p. 17.

34. P. Chung & S. Szklaraki-Smialowska, Corrosion, Vol. 37, No. 1, p. 39.

35. V. Cihal, Corrosion Sci., Vol. 20, 1980, p. 737.

36. E. A. Loria, J. of Metals, Dec. 1979, p. 163.

37. M. Parvizi-Majidi & M. Streicher, Corrosion/82, NACE, Paper 183, April 1982.

38. W. O. Binder, C. M. Brown and R. Franks, Trans. ASM, Vol. 41, 1949, p. 1301.

39. W. L. Clarke, R. L. Cowan, R. Franks, and W. L. Walker, ASTM STP 656, 1978, p. 95.

40. A. A. Babakor, Yu. V. Zakhorov, F. L. Levin & A. T. Colovin, Zaskchita Metallov., Vol. 5, 1969, p. 332.

41. L. Ljungberg, EPRI Workshop on Low Temp. Sensitization, P. per No. 5, January 1982.

42. T. Fukuzuka et al., Proc. Seminar on Countermeasures for Pipe Cracking in BWRs, EPRI WS-79-174, May 1980, Paper 46.

43. S. Nagata, Proc. Seminar on Countermeasures for Pipe Cracking in BWRs, EPRI WS-79-174, May 1980, Paper 43.

44. T. Kobayashi, Proc. Seminar on Countermeasures for Pipe Cracking in BWRs, EPRI WS-79-174, May 1980, Paper 44.

45. M. Kowaka, et al., in Predictive Methods for Assessing Corrosion Damage to BWR Piping & PWR Steam Generators, ed. H. Okada and R. Staehle, NACE 1982, p. 193.

46. K. Fujiwara, T. Fukuzoka, K. Shimagari, and H. Tomari, in Predictive Methods for Assessing Corrosion Damage to BWR Piping & PWR Steam Generators, ed. H. Okada and R. Staehle, NACE 1982, p. 187.

47. S. Iwasaki, in Predictive Methods for Assessing Corrosion Damage to BWR Piping & PWR Steam Generators, ed. H. Okada and R. Staehle, NACE 1982, p. 144.

48. T. Kowakubo, et al., Proc. of Symposium Corr. & Stress Corr., Japan Inst. of Metals, 1977.

49. M. Akashi & T. Kawamoto, IHI Eng. Reviews, Vol. 11, No. 1, 1978.

50. F. Umemura, et al., IHI Eng. Rev., Vol. 6, No. 2, 1983.

51. M. Kowaka, in Predictive Methods for Assessing Corrosion Damage to BWR Piping & PWR Steam Generators, ed. H. Okada and R. Staehle, NACE 1982, p. 205.

52. Kuriboyaski & Okaboyaski, J. Japan Inst. of Metals, Vol. 46, No. 6, 1982, p. 626.

53. Aaltonen, et al., Corr. Sci., Vol. 23, No. 4, 1983, p. 431.

54. C. H. Samans, Corrosion, Vol. 20, 1964, p. 256(t).

55. C. L. Briant, Corrosion, Vol. 38, No. 11, 1982, p. 596.

56. P. Berge & D. T. Noel, EPRI International Workshop on Low Temperature Sensitization, January 1982, Paper No. 2.

57. L. Colombier, "Molybdenum in Stainless Steels and Alloys," Climax Molybdenum Company, Ltd., London, Great Britain, 1967.

58. K. Osozawa and H. J. Engell, Corr. Sci., 6, 1966, p. 389.

59. V. Cihal, "Intergranular Corrosion of Cr-Ni Stainless Steel," presented at Unieux Conference, May 5, 1969.

60. K. L. Money and W. W. Kirk, Mater. Perform., Vol. 9, No. 3, 1970, p. 18.

61. H. S. Armijo, Corrosion, Vol. 24, 1968, p. 24.

62. A. R. Perrin and K. T. Aust, Mat. Sci. and Eng., Vol. 51, 1981, p. 165.

63. A. Joshi and D. J. Stein, Corrosion, Vol. 28, No. 9, 1972, p. 321.

64. H. Coriou, A. Desestret, L. Grall and J. Hochman, Revue de Metallurgie, Vol. 61, 1964, p. 177.

65. H. Coriou, A. Desestret, L. Grall and J. Hochman, Comptes Rendus, Vol. 254, 1964, p. 4467.

66. W. A. T. Clark, T. Arul Mozhi and D. D. MacDonald, 2nd Annual Report, DOE/ER/10972-T2; April 1983.

67. T. M. Divine, C. L. Briant and B. J. Drummond, Scripta Metall., Vol. 14, 1980, p. 1175.

68. J. B. Lumdsen and P. J. Stocker, Scripta Metall., Vol. 15, 1981, p. 1295.

69. C. L. Briant, Corrosion, Vol. 36, 1980, p. 497.

70. S. Danyluk and J. Y. Park, Scripta Metall., Vol. 16, 1982, p. 769.

71. K. T. Aust, Trans TMS-AIME, Vol. 245, 1969, p. 2117.

72. E. D. Hondros and M. P. Seah, Int. Metall. Rev., Vol. 222, December 1977, p. 262.

73. H. Okada, S. Abe, M. Kojima an dY. Hosoi, Proc. of 7th Int. Congress on Metallic Corrosion, Rio De Jenero, September 1978.

74. C. L. Briant and S. K. Banerji, Metall. Trans., Vol. 10A, 1979, p. 1151.

75. F. P. A. Robinson and W. G. Scurr, Corrosion, Vol. 33, No. 11, 1977, p. 408.

76. J. W. Farrell and P. C. Rosenthal, Metal Prog., Vol. 77, 1960, p. 101.

77. V. V. Leviten and V. I. Syreishchikova, Fizikal Met. Metallur., Vol. 7, No. 2 1959, p. 308.

78. J. Voeltzel and G. Henry, Mem. Sci. Rev. Metall., Vol. 61, No. 2, 1964, p. 123.

79. N. V. Baldena, Z. M. Kalina, M. F. Longinor and N. G. Vertii, Met. Sci and Heat Treat., Vol. 15, No. 11-12, 1973, p. 100.

80. D. A. Mortimer, in Grain Boundaries in Engineering Materials, eds. J. L. Walter, J. H. Westbrook and D. A. Woodford, Claiter's Pub. Div., Baton Rouge, LA, 1975, p. 647.

81. T. M. Williams, A. M. Stoneham and D. R. Harris, Met. Sci., Vol, 10, 1976, p. 14.

82. L. Karlsson, H. O. Andren and H. Norden, Scripta Metall., Vol. 16, 1982, p. 297.

83. C. L. Briant and R. A. Mulford, Metall. Trans., Vol. 13A, 1982, p. 745.

84. R. H. Jones, S. M. Bruemmer, M. T. Thomas and D. R. Baer, Scripta Metall., Vol. 16, 1983, p. 615.

85. G. Tauber and H. J. Grabke, Ber. Bung. Phys. Chem., Vol. 82, 1978, p. 298.

86. T. Rosso and C. Sabatini, Scripta Metall., Vol. 6, 1972, p. 51.

87. A. J. Sedriks, Corrosion of Stainless Steels, Wiley Publ. N. Y., 1979.

88. R. W. Staehle, et al., Corrosion, Vol. 26, No. 11, 1970, p. 451.

89. J. E. Alexander, Proc. Seminar on Countermeasures for Pipe Cracking in BWRs, EPRI WS-79-174, May 1980, Paper 48.

90. W. J. Shack, et al., Annual Report October 1981 - September 1982, NUREG/CR-3292, 1983.

91. S. H. Bush et al., Investigation and Evaluation of Stress Corrosion Cracking in Piping of Boiling Water Reactor Plants, NUREG-1061, V. 1, August 1984.

92. H. Hanninen and E. Minni, Metall. Trans., Vol. 13A, 1982, p. 2281.

93. S. Abe and T. Ogawa, Metal. Prog., September 1979, p. 61.

94. L. Kaufman and H. Nesor, Z. Metallk., Vol. 64, 1973, p. 245.

95. M. Hasebe and T. Nishijawa, in Applications of Phase Diagrams in Metallurgy and Ceramics 2, ed. G. C. Carter, NBS Special Publ. 496, 1978, p. 911.

96. H. D. Solomon, Corrosion, Vol. 34, No. 6, 1978, p. 183.

97. H. D. Solomon and D. C. Lord, Corrosion, Vol. 36, No. 8, 1980, p. 395.

APPENDIX A

MEASUREMENT TECHNIQUES FOR DETERMINING SENSITIZATION

APPENDIX A

MEASUREMENT TECHNIQUES FOR DETERMINING SENSITIZATION

In order to assess the effects of individual elements on sensitization, a reproducible and quantitative method is required to measure a material's degree of sensitization (DOS). Five standard corrosion testing methods and several electrochemical testing methods have been used to detect the susceptibility of stainless steels to intergranular attack. The environments and conditions are quite different in these tests, leading to a marked difference in material response. Thus, the understanding of what specific standard each test is measuring is critical in predicting a material's resistance to intergranular attack in a particular service environment. The following sections briefly discuss the capabilities, relative sensitivities, and application to IGSCC in high-temperature water environments of the corrosion and electrochemical test methods available.

A.1 ASTM STANDARD CORROSION TESTS A262-77a[1]

A.1.1 Practice A - Oxalic Acid Etch Test

The oxalic acid test is a quick method for identifying nonsusceptible materials. Specimens which have a nonacceptable etch structure (dual or ditched) must be evaluated by a more quantitative hot corrosion test. This aggressive test environment promotes the dissolution of $M_{23}C_6$ carbides and, perhaps, also attacks the chromium depleted zone along grain boundaries. The major limitation of the oxalic acid test is that it is only a qualitative evaluation and does not supply a quantitative DOS value by which the material's susceptibility can be assessed.

A more quantitative method of examination requires the determination of the fraction of ditched grain boundaries. This method has been shown to give reasonable correlations with other corrosion test techniques. However, since carbides are attacked, it is not possible to directly correlate results with the extent of chromium depletion and measure a quantitative DOS value.

A.1.2 Practice B - Ferric Sulfate-Sulfuric Acid Test

The ferric sulfate-sulfuric acid, or Streicher, test determines material susceptibility to intergranular attack by comparison of weight-loss data to the weight loss of an unsensitized, solution-annealed specimen. Specimens are rejected if the weight loss is more than a certain factor greater than that of the solution-annealed specimen. The presence of ferric salts inhibits the general corrosion of the stainless steel in this solution, but does not prevent attack of $M_{23}C_6$ carbides and chromium-depleted grain boundary regions. It is

also possible that since the Streicher test operates at oxidizing potentials (Figure A.1), impurity segregation (e.g., phosphorus) may also contribute to the intergranular attack.

A.1.3 Practice C - Nitric Acid Test

Weight loss is again used as the measure of DOS in the nitric acid, or Huey, test. Specimens are exposed to boiling 65% nitric acid solution in several steps, and weight loss is measured after each boiling period. Carbides, sigma-phase, and chromium-depleted and phosphorus-segregated regions are strongly attacked in the Huey test. The specimen potential, which starts near the transpassive region of the polarization curve (Figure A.1), increases during the test as Cr^{6+} ions are produced by the corrosion process. Thus, the solution aggressiveness increases over time, and exposure steps are limited to 48-hour periods. The most practical use for the Huey test is screening materials to be used in nitric acid (or other highly oxidizing) environments and not for materials to be used in high-temperature water environments.

A.1.4 Practice D - Nitric-Hydrofluoric Acid Test

The nitric-hydrofluoric acid test was designed to evaluate intergranular attack susceptibility of molybdenum-bearing grades of austenitic stainless steels. Corrosive attack in this solution is very sensitive to bulk and localized variations in chromium content. It has been used with success in measuring sensitization of Types 316 and 316L stainless steels.[2] This test has not been used extensively because both Practices B and E supply similar results, and because of the difficulty in handling a test solution containing hydrofluoride acid.

A.1.5 Practice E - Copper Sulfate-Sulfuric Acid Test

The final standard corrosion test is also the most sensitive to chromium-depleted zones in austenitic stainless steels. Evidence indicates that chromium-depleted zones are selectively dissolved before carbides and matrix regions. A key accelerant in the copper sulfate-sulfuric acid, or Strauss, test is the presence of metallic copper in solution with the stainless steel specimen. Copper accelerates intergranular attack of stainless steel by reducing and stabilizing its potential near the active-passive transition region, as shown in Figure A.1. At this potential, the dissolution rate for chromium-depleted areas is significantly greater than for the matrix.

Several methods have been used to evaluate DOS from Strauss test results. Depth penetration measurements (after bending) have been a common method of

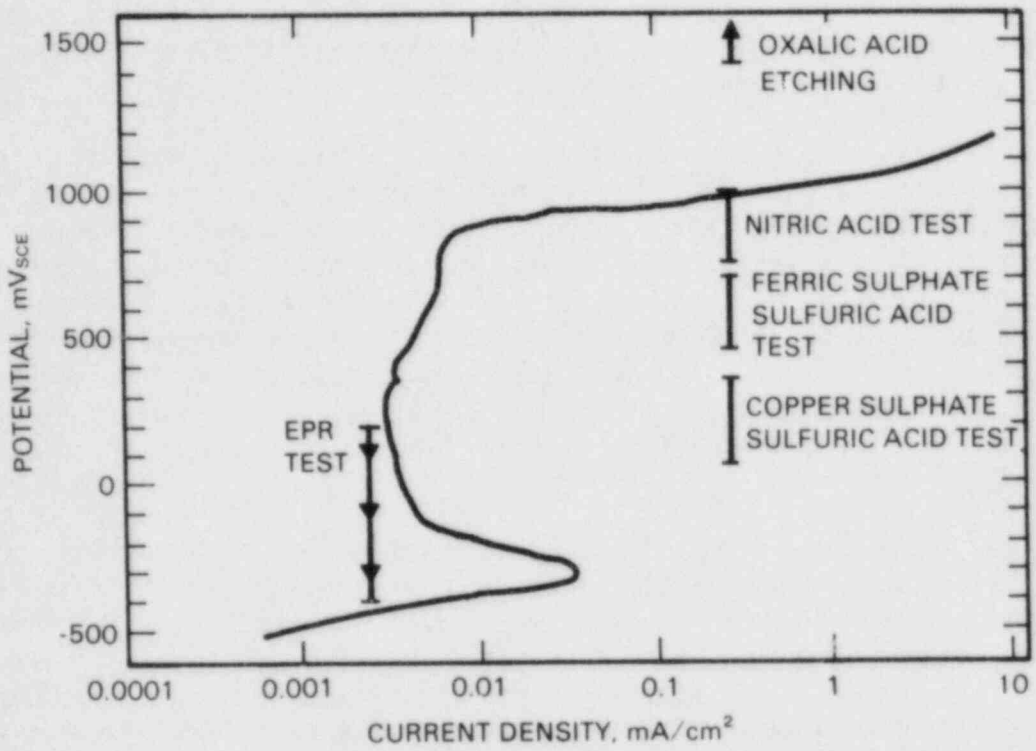

FIGURE A.1. Corrosion Potential Regions for Austenitic Stainless Steels in Intergranular Corrosion Test Solutions

quantitatively determining DOS. Perhaps the most limiting aspect of the Strauss test is the time required for testing. Several 72-hour exposures may be required to evaluate materials with low DOS values.

A.2 ELECTROCHEMICAL POTENTIOKINETIC REACTIVATION TESTS

The passive film that forms on stainless steels depends on the material's chromium concentration and the environment. Localized areas sufficiently depleted in chromium will form films less protective than areas of high chromium. This basic principle governs the application of the electrochemical potentiokinetic reactivation (EPR)[3-6] test for measuring DOS. Reactivation from the passive state leads to local film breakdown and attack of chromium-depleted zones. If a material is nonsensitized, the passive film will remain intact for much longer times during reactivation and suppress the large active peak observed during anodic polarization or during reactivation of a severely sensitized specimen.

The measurement of specimen DOS has most commonly been based on the charge transfer between the metal and electrolyte during the potentiokinetic reactivation[3] or as a ratio of this value to the charge transfer accumulated during

an anodic scan.[6] Measured values depend on a variety of test, environment, and material parameters, which must be kept constant to properly assess material susceptibility to intergranular attack.

The EPR test offers many advantages over the standard corrosion tests described in Section A.1. With the exception of the oxalic acid test, the ASTM recommended practices are destructive and time consuming tests, and none of the standard tests can be readily used to give quantitative measurements of the susceptibility to intergranular attack. The EPR test, on the other hand, is a rapid and nondestructive method of determining susceptibility. It is particularly useful in discriminating among materials with low to moderate sensitization levels. EPR DOS measurements have shown good agreement with Strauss test results and with IGSCC susceptibility in high-temperature water environments.[3-6]

Several other electrochemical test techniques[7,8] in solutions similar to that used in EPR tests have produced comparable results. Anodic polarization and constant-potential etching tests determine DOS by measuring the current density (or charge transfer) at a particular potential in the active-passive region. This potential corresponds to the location of a second anodic peak[7] that is dependent on dissolution of chromium-depleted regions. However, the standard EPR test is currently far more advanced in understanding and correlation to service experience.

A.3 DIRECT MEASUREMENT OF CHROMIUM DEPLETION

The susceptibility of austenitic stainless steels to intergranular corrosion and SCC is caused by the precipitation of chromium-rich carbides and the localized depletion of chromium in adjacent regions. This conclusion has largely resulted from direct observation of carbide precipitation and indirect (corrosion-type) inference of a chromium-depleted zone. However, with the development of scanning transmission electron microscopy with energy-dispersive X-ray spectroscopy (STEM-EDS), many direct measurements of chromium concentration profiles at grain boundaries have been reported.[9-13] An example of the gradient in chromium content that is observed when traversing a grain boundary in a sensitized stainless steel is shown in Figure A.2.

Material DOS depends both on the minimum chromium composition at the grain boundary and the width of the depleted zone. The true minimum chromium composition at the grain boundary or carbide interface cannot normally be measured by STEM-EDS since the analysis volume is too large. Thus, the boundary analysis is an average of the boundary and considerable matrix region as well. Minimums measured at grain boundaries in sensitized material are typically about 10 wt% chromium while thermodynamic considerations[14] suggest the minimum to be closer to 8 wt%. The width of the chromium-depleted zone, on the other hand, can be measured accurately for moderately to severely sensitized

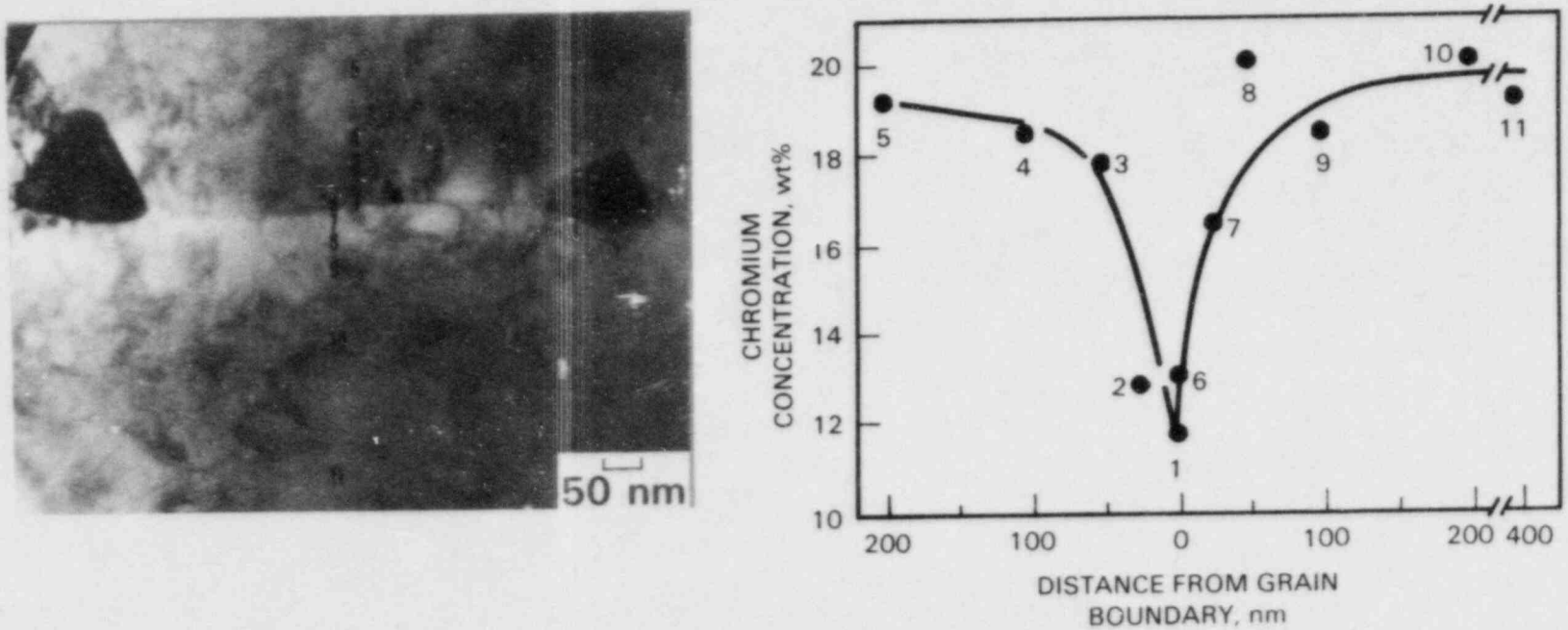

FIGURE A.2. Chromium Depletion Profile Across Grain Boundary in Sensitized 304 Stainless Steel

material because it is greater than the technique resolution. The practical resolution for most STEM-EDS analysis is on the order of 100 Å due to beam broadening effects. Measured grain boundary chromium-depleted zone widths in Types 304 and 316 SS have ranged from less than 100 Å for slightly sensitized material to more than 6000 Å for severely sensitized material. These widths are of the same order as those predicted by the theoretical models of Stawström and Hillert[15] and Tedmon et al.[14]

There have been very few studies using higher spatial resolution (atom-probe field-ion microscopy) or surface-sensitive (Auger electron spectroscopy) techniques to measure grain boundary chromium compositions and chromium profiles. Henjered et al.[16] compared STEM-EDS measurements on a sensitized titanium stabilized stainless steel to those obtained using a field-ion microscope. Surprisingly, atom-probe field-ion microscopy revealed chromium levels of less than 4% at the grain boundary. Auger electron spectroscopy measurements of grain boundaries in sensitized Type 304 SS fractured within the high-vacuum system revealed chromium levels of about 8 wt% in one study[17] and more than 11 wt% in another.[18]

A.4 APPLICABILITY OF SENSITIZATION MEASUREMENT TECHNIQUES TO PREDICT IGSCC SUSCEPTIBILITY

The ultimate usefulness of the measurement techniques discussed in this section is judged by their ability to predict IGSCC susceptibility. For the purposes of this study, the environment of interest is high-temperature water. The modified Strauss and EPR tests appear to be the most accurate in assessing chromium depletion in stainless steels. As a result, these two techniques are the most likely to predict IGSCC susceptibility. In recent years, several studies have been performed to correlate these techniques (and others) to actual SCC test results. DOS predictions by modified Strauss and EPR tests are consistent with cracking susceptibility in constant extention rate (CERT), constant load, creviced bent beam, and U-bend tests. Examples of the correlation between evaluation and SCC tests are presented in Figure A.3.

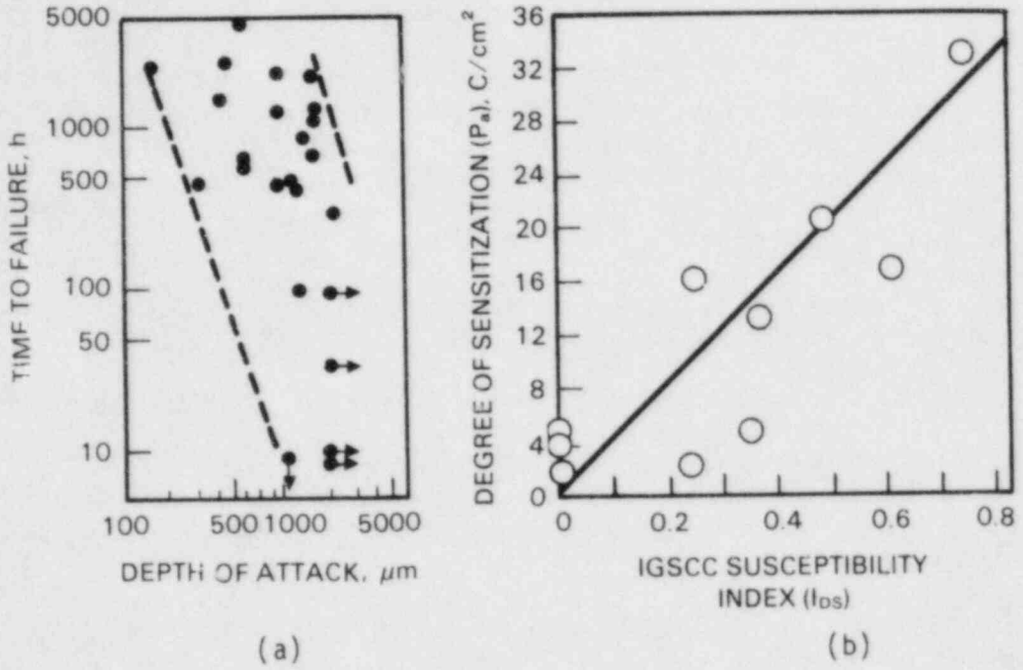

FIGURE A.3. Correlations Between DOS and SCC Susceptibility Measurements: (a) Strauss Test Versus Failure Time in Constant Load Test[19] and (b) EPR Test Versus CERT Results[4]

REFERENCES

1. Standard Practices for Detecting Susceptibility to Intergranular Attack in Austenitic Stainless Steels, A262-81, in 1981 Annual Book of ASTM Standards Section 1, ASTM, Philadelphia, PA, 1984, p. 66.

2. D. Warren, ASTM Bulletin, May 1958, p. 45.

3. W. L. Clarke, General Electric Report GEAP-21382, U.S. Nuclear Regulatory Commission NUREG-0251-1, August 1976.

4. W. L. Clarke, R. L. Cowan and W. L. Walker, in ASTM STP 656, 1978, p. 99.

5. V. Cihal, Corr. Sci., Vol. 20, 1980, p. 737.

6. F. Umemura, Y. Hanai and T. Kawamoto, IHI Eng. Rev., Vol. 6, No. 2, 1983, p. 1.

7. P. Chung and S. Szklarska-Smialowska, Corrosion, Vol. 37, No. 1, 1981, p. 39.

8. J. C. Charbonnier and T. Jossic, Corr. Sci, Vol. 23, No. 11, 1983, p. 1191.

9. E. L. Hall and C. L. Briant, Metall. Trans., Vol. 15A, 1984, p. 793.

10. C. A. Pande, M. Suenaga, B. Vyas, H. S. Isaacs and D. F. Harling, Scripta Metall., Vol. 11. 1977, p. 681.

11. M. G. Lackey and F. J. Humphreys, Proceedings of the 3rd Int. Conf. on Effect of Hydrogen on Behavior of Materials. Edited by I. M. Bernstein and A. W. Thompson, AIME, 1981, p. 665.

12. T. Thorvaldsson and G. L. Dunlop, J. of Mat. Sci., Vol. 18, 1983, p. 793.

13. L. Ljungberg, EPRI Workshop on Low Temp. Sensitization, January 1982, Paper No. 5.

14. C. S. Tedmon, Jr., D. A. Vermilyea and J. H. Rosolowski, J. Electrochem. Soc., Vol. 118, 1971, p. 1971.

15. C. Stawström and M. Hillert, J. Iron and Steel Inst. January 1969, p. 77.

16. A. Henjered, N. Norden, T. Thorraldsson and H.-O. Ardren, Scripta Metall., Vol. 17, 1983, p. 1275.

17. J. B. Lumsden and P. J. Stocker, Scripta Metall., Vol. 15, 1981, p. 1295.

18. S. Abe and T. Ogawa, Metal Prog., Sept 1979, p. 61.

19. S. Hattosi, et al., in Predictive Methods for Assessing Corrosion Damage to BWR Piping and PWR Steam Generator, ed. H. Okada and R. Staehle, NACE 1982, p. 215.

APPENDIX B

METHOD TO DETERMINE FACTOR OF IMPROVEMENT IN SENSITIZATION RESISTANCE FROM MATERIAL COMPOSITION

APPENDIX B

METHOD TO DETERMINE FACTOR OF IMPROVEMENT IN SENSITIZATION RESISTANCE FROM MATERIAL COMPOSITION

Sensitization of an austenitic stainless steel refers to an increased susceptibility to intergranular attack due to the precipitation of chromium-rich carbides at grain boundaries. This precipitation and the significant difference in diffusivities of chromium and carbon leads to the formation of a chromium-depleted zone. The depleted region can be electrochemically "active" relative to the matrix depending on the depth and width of the chromium concentration gradient. As a result, preferential intergranular corrosion and/or SCC can occur.

The sensitization and IGSCC susceptibility potential of any heat of material is primarily controlled by its bulk composition. The effects of individual elements on sensitization can, therefore, be determined by comparison with experimental data. Cihal[1] initially proposed compositional equivalency parameters to correlate heat-to-heat property variations. The basic premise still holds in that a relatively simple equation can be used to assess a material's sensitization propensity. In the review, many equivalency formulations were assessed by comparison with a large sensitization data base. Model predictions were correlated with experimental time-to-sensitize measurements. The best fit to experimental data was achieved using a slightly modified version of the Cihal[1] elemental parameters:

$$Cr^* = Cr + 1.6\ Mo - 0.2\ Ni - 100\ C \qquad (B.1)$$

where Cr* is the composite chromium content and is related to the equilibrium chromium content adjacent to a $M_{23}C_6$ carbide, and all concentrations are expressed as weight percentages. The correlation between time-to-sensitize data and prediction is shown graphically in Figure B.1. A linear regression analysis of all data resulted in the equation:

$$\log_{10}(t_s) = -3.96 + 0.325\ Cr^* \qquad (B.2)$$

or

$$\ln(t_s) = -9.108 + 0.748\ Cr^* \qquad (B.3)$$

where t_s equal the time to sensitize in hours. It is important to note from Figure B.1 that the scatter in time-to-sensitize data for a particular Cr* is as much as two orders of magnitude. This scatter is due to many factors including variations in initial material condition, differences in experimental

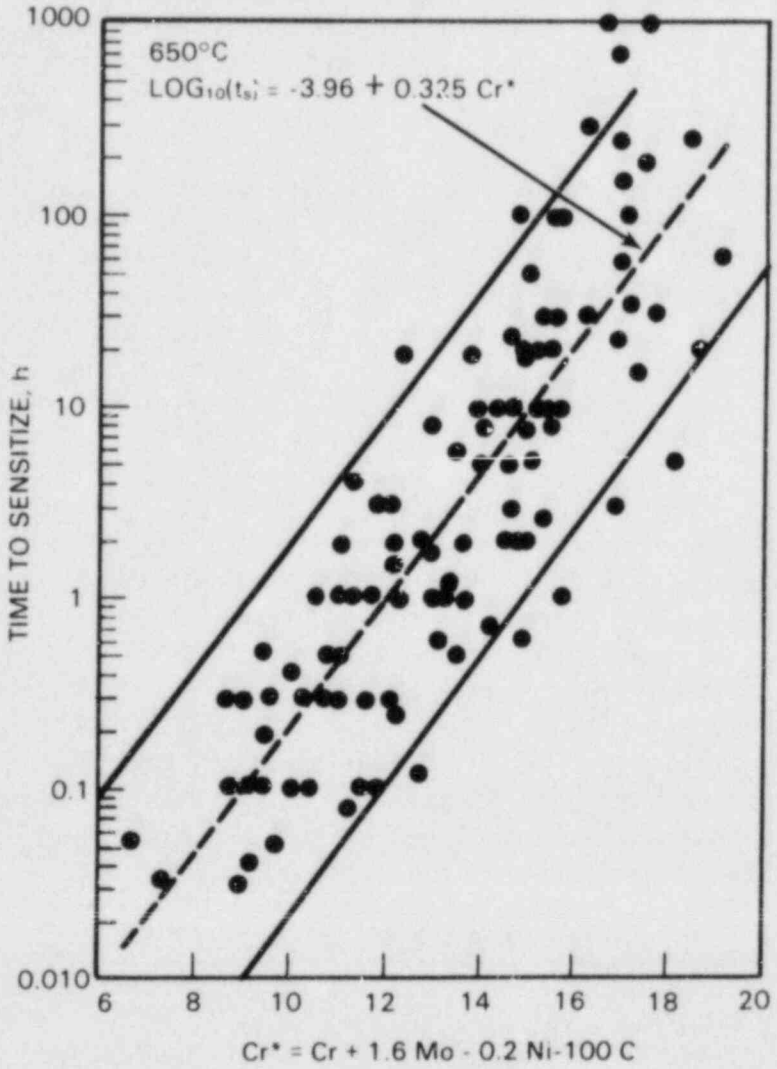

FIGURE B.1. Correlation Between Composition Normalization Parameter, Cr*, and Experimentally Measured Time-to-Sensitize Data

techniques among laboratories, and the difficulty in identifying the time to sensitize from the reported data. Thus, although the prediction equation fits the trend of the data set, it cannot be used for quantitative prediction of sensitization times.

The relationship depicted in Equation B.2 allows the prediction of sensitization propensity as a function of material composition. To compare various heats of material, the factor of improvement (F/I) in time-to-sensitize of heat 1 over heat 2 is obtained using Equation B.3 by the ratio:

$$F/I = \frac{\exp\ (-9.108 + 0.748\ Cr_1^*)}{\exp\ (-9.108 + 0.748\ Cr_2^*)} \qquad (B.4)$$

where Cr_1^* is the composite chromium value of heat 1 and Cr_2^* is the composite chromium value of heat 2.

Examples of these factors of improvement in comparison to a high-carbon and a standard Type 304 SS are listed in Table B.1 for Types 304, 304L, 304NG, 316, 316L and 316NG stainless steels. The significant effect of reducing carbon content is observed by comparing improvement factors with a particular alloy type, either Type 304 or 316 SS. A factor of improvement of 20 is predicted for Type 316NG over standard Type 304 SS.

Although time-to-sensitize data were obtained from tests on isothermally heat-treated specimens, the data do indicate relative improvements expected in weld-induced sensitization. Thermomechanical cycling during welding has been shown to accelerate sensitization development. Thus, the calculated time to sensitize will be an overestimation of the actual HAZ time to sensitize. The factor of improvement will also be changed, but may still reflect the relative magnitude noted for the isothermal case. Verification tests are required to determine and document whether such a correlation is possible.

TABLE B.1. Calculated Sensitization Times (t_s) and Factors of Improvement (F/I) for Several Types 304 and 316 Stainless Steels

Alloy	Composition, wt% C	Cr	Ni	Mo	Cr*, %	Time to Sensitize (t_s), h	Factor of Improvement (F/I) High Carbon	Standard Carbon
304	0.08	18.5	8.5	0.2	9.12	0.10	1	0.1
304	0.05	18.5	8.5	0.2	12.12	0.96	10	1
304L	0.035	18.5	8.5	0.2	13.62	2.94	29	3
304NG	0.02	18.5	8.5	0.2	15.12	9.04	90	9
316	0.08	17	12.5	2.2	10.02	0.20	2	0.2
316	0.05	17	12.5	2.2	13.02	1.88	19	2
316L	0.035	17	12.5	2.2	14.52	5.77	58	6
316NG	0.02	17	12.5	2.2	16.02	17.73	177	18

REFERENCES

1. V. Cihal, Intergranular Corrosion of Cr-Ni Stainless Steel, presented at Unieux Conference, May 5, 1969.

DISTRIBUTION

No. of Copies

OFFSITE

U.S. Nuclear Regulatory Commission
Division of Technical Information and Document Control
7920 Norfolk Avenue
Bethesda, MD 20014

J. Muscara
Materials Engineering Technology Division
Nuclear Regulatory Commission
Mail Stop 5650NL
Washington, DC 20555

E. F. Rybicki
Mechanical Engineering Dept.
University of Tulsa
600-South College Ave.
Tulsa, OK 74104

H. D. Solomon
Materials Characterization Laboratory
Corporate Research & Development
General Electric Company
P.O. Box 8
Schenectady, NY 12301

W. E. Wood
Oregon Graduate Center
19600 N.W. Walker Road
Beaverton, OR 97006

No. of Copies

C. L. Briant
General Electric Company
Research and Development Center
P.O. Box 8
Schenectady, NY 12301

E. Merrick
Division of Engineering Design
Tennessee Valley Authority
400 Commerce Avenue
W10-B119C-K
Knoxville, TN 37902

W. J. Shack
Materials Science Division
Argonne National Laboratory
9700 South Cass Avenue
Argonne, IL 60439

J. Y. Park
Materials Science Division
Argonne National Laboratory
9700 South Cass Avenue
Argonne, IL 60439

P. S. Maiya
Materials Science Division
Argonne National Laboratory
9700 South Cass Avenue
Argonne, IL 60439

W. L. Clarke
Vallecitos Nuclear Center
Mail Code V36
Pleasanton, CA 94566

No. of
Copies

J. D. Gilman
Nuclear Power Division
Electric Power Research
Institute
3412 Hillview Avenue
Palo Alto, CA 94304

W. J. Childs
Nuclear Power Division
Electric Power Research
Institute
3412 Hillview Avenue
Palo Alto, CA 94304

K. W. Mahin
Lawrence Livermore Laboratory
University of California
P.O. Box 808
L-2A
Livermore, CA 94550

D. Cubicciotti
Nuclear Power Division
Electric Power Research
Institute
3412 Hillview Avenue
Palo Alto, CA 94304

J. F. Key
Fuels & Materials Division
EG&G Idaho, Inc.
P.O. Box 1625
Idaho Falls, ID 83401

R. Horn
General Electric Company
Nuclear Energy Engineering
Division
175 Curtner Ave.
San Jose, CA 95125

No. of
Copies

P. Lindsey
Bechtel Power Corporation
Mail Stop 62/6/B/6
50 Beale Street
San Francisco, CA 94119

50 Pacific Northwest Laboratory

D. G. Atteridge (5)
S. M. Bruemmer (15)
L. A. Charlot (5)
R. A. Clark
R. L. Clark
E. L. Courtright
S. D. Dahlgren
C. R. Hann
P. E. Hart
E. I. Husa
R. H. Jones
R. S. Kemper
R. F. Klein
R. J. Kurtz
N. J. Olson
T. E. Page (2)
J. L. Pilger
S. G. Pitman
F. A. Simonen
P. L. Whiting
Publishing Coordination (2)
Technical Information (5)

NRC FORM 335 (11-81)

U.S. NUCLEAR REGULATORY COMMISSION

BIBLIOGRAPHIC DATA SHEET

1. REPORT NUMBER (Assigned by DDC)
NUREG/CR-3918
PNL-5186

4. TITLE AND SUBTITLE (Add Volume No., if appropriate)
COMPOSITIONAL EFFECTS ON THE SENSITIZATION OF AUSTENITIC STAINLESS STEELS

2. (Leave blank)

3. RECIPIENT'S ACCESSION NO.

7. AUTHOR(S)
S. M. Bruemmer, L. A. Charlot, D. G. Atteridge

5. DATE REPORT COMPLETED
MONTH: September YEAR: 1984

DATE REPORT ISSUED
MONTH: December YEAR: 1984

9. PERFORMING ORGANIZATION NAME AND MAILING ADDRESS (Include Zip Code)
Pacific Northwest Laboratory
P. O. Box 999
Richland, Washington 99352

6. (Leave blank)

8. (Leave blank)

12. SPONSORING ORGANIZATION NAME AND MAILING ADDRESS (Include Zip Code)
Division of Engineering Technology
Office of Nuclear Regulatory Research
U. S. Nuclear Regulatory Commission
Washington, DC 20555

10. PROJECT/TASK/WORK UNIT NO.

11. FIN NO.
B2449

13. TYPE OF REPORT

PERIOD COVERED (Inclusive dates)
January - September 1984

15. SUPPLEMENTARY NOTES

14. (Leave blank)

16. ABSTRACT (200 words or less)

Pacific Northwest Laboratory is conducting a program, sponsored by the U.S. Nuclear Regulatory Commission, to develop validated models for the prediction of stress corrosion cracking susceptibility in the heat-affected zone of stainless steel weldments. This report reviews the effects of alloying and impurity elements on the sensitization propensity of Types 304 and 316 stainless steel. As expected, carbon was found to be the dominant element controlling sensitization, with chromium, molybdenum, and nickel also important. Other alloying elements, such as manganese and silicon, have at most only a small effect on sensitization. However, strongly segregating elements, such as nitrogen, boron, and phosphorus, may have a significant effect on intergranular corrosion and stress corrosion cracking susceptibility.

17. KEY WORDS AND DOCUMENT ANALYSIS
austenitic stainless steel
stress corrosion cracking
light-water reactor

17a. DESCRIPTORS
chromium-depleted zone
grain boundary segregation

17b. IDENTIFIERS/OPEN-ENDED TERMS

18. AVAILABILITY STATEMENT
Unlimited

19. SECURITY CLASS (This report)
Unclassified

21. NO. OF PAGES

20. SECURITY CLASS (This page)

22. PRICE
$

NRC FORM 335 (11-81)

UNITED STATES
NUCLEAR REGULATORY COMMISSION
WASHINGTON, D.C. 20555

LIGHT WATER REACTOR(LWR) SERVICE

DECEMBER 1984